Processing-Performance Evolution of Perovskite Solar Cells: From Large Grain Polycrystalline Films to Single Crystals

Processing-Performance Evolution of Perovskite Solar Cells: From Large Grain Polycrystalline Films to Single Crystals

Md Azimul Haque, Joel Troughton, Derya Baran**

M. A. Haque, Dr. J. Troughton, Prof. D. Baran
King Abdullah University of Science and Technology (KAUST), Division of Physical Sciences and Engineering (PSE), KAUST Solar Center (KSC), Thuwal, Saudi Arabia
E-mail: derya.baran@kaust.edu.sa, azimul.mohammed@kaust.edu.sa

Keywords: perovskite, grain, single crystal, solar cell

Abstract

Solution-processable halide perovskites have emerged as strong contenders for next-generation solar cells owing to their favorable optoelectronic properties. To maintain the efficiency momentum of perovskite solar cells (PSCs), development of advanced processing techniques, particularly for the perovskite layer, is imperative. There is a close correlation between the quality of the perovskite layer and its photophysical properties: Highly crystalline large grains with uniform morphology of the perovskite layer and their interface with charge transporters are crucial for achieving high performances. Significant efforts have been dedicated to achieve perovskite films with large grains reaching the millimeter-scale for high-efficiency PSCs. Recent work showcase a transition from large grain polycrystalline to single-crystalline (SC) PSCs made possible by the facile growth of perovskite single crystals. In this review, we focus on the recent progress of the large grain polycrystalline PSCs and grain boundary-free SC-PSCs. We highlight the recent approaches of depositing large-grained perovskite layers and single crystal growth techniques adopted for fabrication of efficient PSCs. In addition, prospects of SC-PSCs and their further development in terms of efficiency, device design, scalability, and stability are discussed.

1. Introduction

The emergence of hybrid perovskites has revolutionized the field of solar cell research. Within a decade since the first report on perovskite solar cells (PSCs) appeared, the single junction power conversion efficiency (PCE) has reached a record value of 25.2%.[1] The low-temperature processing of hybrid perovskites along with their favorable optoelectronic properties such as high absorption coefficient, long carrier diffusion lengths, tunable bandgap, and low trap density makes them highly suited for solar cell applications.[2-9] Photophysical properties such as light harvesting efficiency, carrier transport, and diffusion length are closely correlated with crystallinity of the perovskite layer.[10] As such, dense, uniform, and highly crystalline perovskite layers are a prerequisite for high performance solar cells. There have been many strategies developed for achieving high quality pin-hole free perovskite films, including solvent engineering, co-evaporation, vapor assisted solution processing, and so on.[11-13] Besides, there have been also efforts to improve the device design and exploration of different charge transport layers to improve the efficiency.[14] In terms of device innovation, electron/hole transport layer (ETL/HTL) free PSCs and PSCs based on large grain films and single crystals have attracted considerable interest recently.[15-17]

The facile and low-temperature growth techniques of perovskite single crystals (SC) are particularly interesting for fabrication of SC-PSCs as trap states at grain boundaries in polycrystalline films aid in the non-radiative recombination of carriers, limiting the performance of PSCs.[18] One other major advantage of large grain perovskite films and grain boundary-free single crystals is the possibility of achieving better charge transport, device performance, and stability owing to the reduction of grain boundaries. In addition, single crystals extend this line of thinking to offer the possibility of probing issues of ambient stability, ion migration, and

hysteresis in the most intrinsic form. It was recently observed that polycrystalline film based PSCs exhibit facet dependent photovoltaic performance.[19] The intra-grain heterogeneity in the photovoltaic parameters suggests orientational dependent defect concentrations which have a direct implication on macroscale device performance. In general, single crystals have better homogeneity and low defects than their polycrystalline counterparts which is particularly beneficial for high performance optoelectronic devices. In the initial years after the first report on PSCs, apart from studying the single crystals for crystallographic information and charge transport properties, single crystals of perovskite were also explored as optical sensors.[20-22] In recent years, with the development of facile growth techniques for perovskite single crystals, high performance SC-PSCs and X-ray detectors have been developed.[17,23-24]

The facile solution-processed nature and tunability of hybrid perovskites have led to a large number of studied compositions. Aside from solar cells, the extraordinary optoelectronic properties of perovskites have led to many other exciting applications including UV-Vis photodetectors, X-ray detectors, lasing and light emitting diodes (LEDs).[20,25-27] Hybrid perovskites are classified as perovskite, given they share the same ABX_3 crystal structure as the "original" perovskite - $CaTiO_3$. The flexibility of the hybrid perovskite lattice offers the opportunity to replace the A, B, and X sites with different elements, resulting in a large number of different compositions (**Figure 1**). The most common 3D hybrid perovskite consists of a methylammonium (MA) cation at the A-site, lead (Pb) at the B-site, and halides (I, Br, Cl) at the X-site. Other popular hybrid perovskites are formed by replacing MA with formamidinium (FA) organic cations. There are also all-inorganic halide perovskites where the A-site is occupied by Cesium (Cs) and mixed cation perovskites where A-site has combination of cations.[28-29]

Recently, mixed B-site perovskites have also started to attract attention due to their enhanced stability.[30]

Pb-free hybrid perovskites such as $ASnX_3$ (A= MA, FA, Cs; X=I, Br., Cl) have also attracted significant interest for solar cells given their comparatively narrower band gaps,[31-32] but often suffer from poor stability in air due to oxidation of Sn. Recently, mixed perovskites have been reported to have enhanced stability compared to single phase. Mixed perovskites generally have multiple A-site cation and X-site halides. There are also low dimensional analogues of 3D perovskites such as so-called "2D" and "0D" hybrid perovskites. While there have been few reports on solar cells based on these low-dimensional perovskites, their power-conversion efficiencies are generally lower than 3D counterparts due to constrained charge transport. It is interesting to note that the 3D to 2D transitions can be achieved by changing the organic cation to a larger one.[33] In this review, we will mostly discuss hybrid and mixed perovskites as most of the work on large grain polycrystalline PSCs and SC-PSCs are based on hybrid/mixed perovskites.

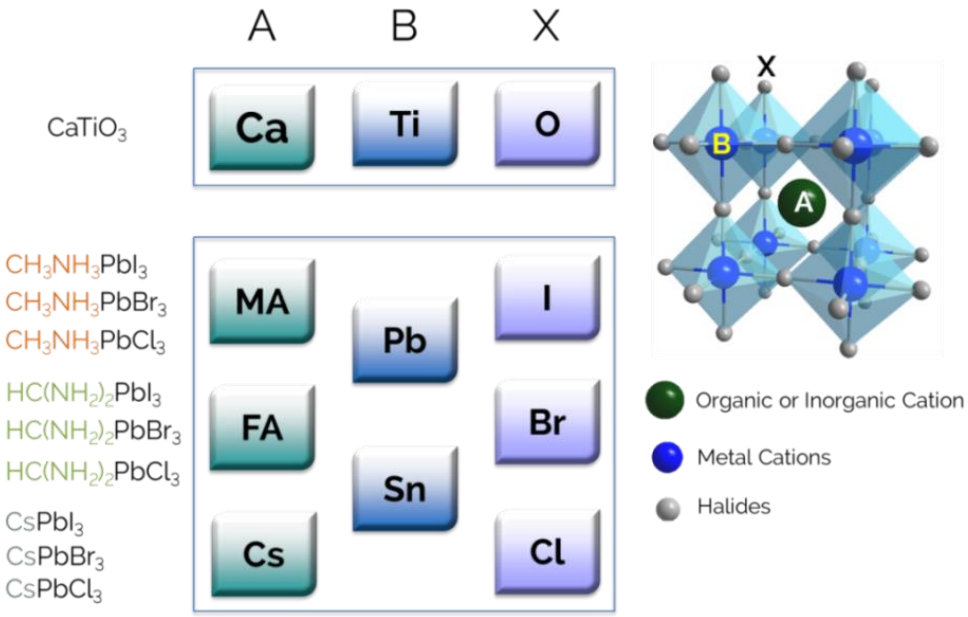

Figure 1. ABX_3 perovskite structure and different possible compositions depending on the cations and anions.

The optical bandgap in hybrid perovskites can be tuned from visible to UV region by manipulating the halide composition. For $MAPbX_3$, the bandgap increases upon the substitution of iodide with chloride. Such bandgap tunability is particularly interesting for devices such as photodetectors, lasers, and LEDs. In terms of electronic defects, hybrid perovskites are known to be defect-tolerant and exhibit low trap densities. In one early work[4], Bakr et al. grew $MAPbI_3$ and $MAPbBr_3$ single crystals and found that the trap densities were in the range of 10^9-10^{10} cm^{-3}. In another work by Haung et al., diffusion lengths for carriers was observed to be greater than 175 μm in $MAPbI_3$.[7] Such low trap densities and long diffusion lengths, combined with high absorption coefficients, contribute to the high efficiency of PSCs.

In this review, we focus on the work with PSCs based on large grain polycrystalline films and single crystals. A general overview of polycrystalline perovskite films and some key strategies developed to fabricate large grain polycrystalline perovskite films, and their relevant photovoltaic performances are discussed in Section 2. Section 3 summarizes the techniques for growing perovskite single crystals as well as vertical and lateral structure SC-PSCs. Finally, in Section 4, we discuss the limitations and prospects of PSCs.

2. Polycrystalline Perovskite Thin Films: Techniques and Large grain-based PSCs

Among all the micro-morphologies of halide perovskites, the polycrystalline thin film one has been most widely studied owing to an easy fabrication process and great potential in photovoltaic applications.[34] In short, two or more perovskite precursors, i.e., methylammonium halides (I, Br or Cl) and lead halides are combined through solution or vapor approach to yield a resulting perovskite film. The final perovskite film quality, in terms of its morphology and grain

size, is greatly affected by the processing conditions. The average perovskite grain sizes in early works were typically below 500 nm. With the advent of new processing techniques, the grain sizes have reached to micro and millimeter scale. **Figure 2** shows some representative techniques of perovskite thin film deposition.

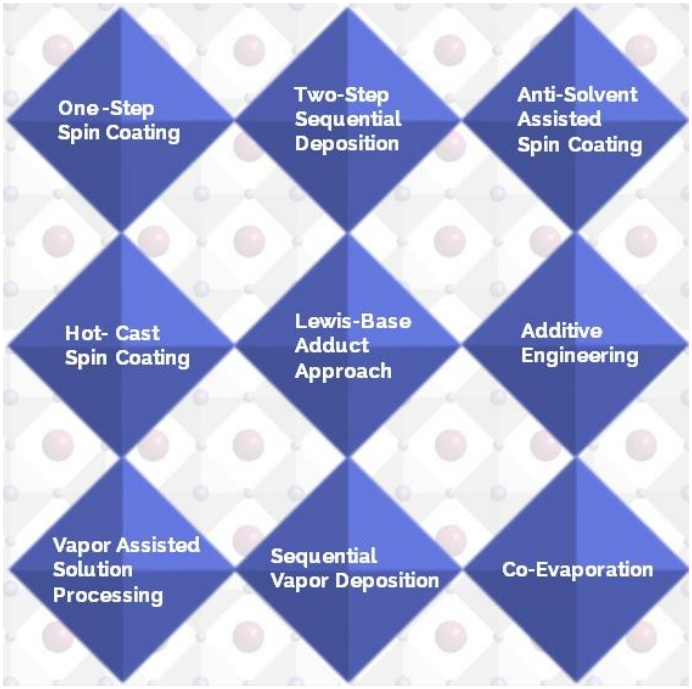

Figure 2. Various methods of growing polycrystalline hybrid perovskite films.[12-13,35-42]

Solution-based processing is the most popular approach in terms of perovskite film fabrication. Typically, in "one-step" spin coating method, MAX and PbX_2 (X = I, Br, or Cl) are fully dissolved in an organic solvent or mixture of solvents (e.g. DMF, DMSO GBL) and then directly spin-coated onto the substrate. In one early report, Snaith and co-workers fabricated "meso-superstructured solar cell" with an efficiency of 10.9% by one-step spin coating method.[43] Later, Seok et al. developed solvent-engineering technology to form extremely uniform and dense perovskite layers.[11] During the spinning process, toluene which does not dissolve the perovskite, was dripped above the sample surface, and a high efficiency of 16.2%

was achieved. While initial work relied mostly on one-step spin coating, the prevalence of pinholes within the resulting film made the fabrication of planar perovskite solar cells difficult given contact between charge transport layers. However, with the advent of planar perovskite solar cells, it became necessary to either modify the existing solution processing or develop new techniques to achieve pinhole-free perovskite layers. The rise in popularity of the solvent-engineering approach has allowed easier fabrication of perovskite films for planar junction applications.

Aside from solution processing, vapor-based techniques have also been extensively adopted by the researchers. In an early work, Snaith and co-workers[12] adopted a dual-source thermal evaporation system. The organic source (MAI) and inorganic source ($PbCl_2$) were co-evaporated on to the sample to form a continuous and uniform perovskite layer with larger grains compared to routine solution-processed layers. This co-evaporation technique was reported earlier, in 1997, by Tsutsui et al. for the deposition of $MAPbI_3$ using PbI_2 and MAI as sources.[44] Somewhat different from solution and vapor-based deposition, Yang Yang and coworkers demonstrated a method of vapor-assisted solution processing (VASP) for fabricating smooth perovskite thin films.[13] The process involved a solution-based process to form an inorganic PbI_2 film first which was subsequently treated with the desired organic vapor (MAI). This method takes advantage of the kinetic reactivity of MAI and thermodynamic stability of perovskite during the in situ growth process and provides films with well-defined grain structure with grain sizes up to the microscale.

The rationale behind developing large grain perovskite films was to reduce the diminished optical and electronic properties of small grains and grain boundaries, limiting the efficiency of PSCs. In one early report, it was found that small perovskite crystallites suppress exciton

formation.[45] In addition, trap densities at grain boundaries can severely affect carrier diffusion leading to nonradiative recombination.[46] Also, issues of ambient stability and ion migration have been linked to the defects present at grain boundaries. Accelerated degradation of perovskite films, under humid conditions, occurs preferentially along grain boundaries compared to grain surfaces, suggesting that reducing the number of grain boundaries will be a step towards improving the stability of perovskite devices.[47] In a recent work, a comparative study between microstripes, thin film, and single crystal of $MAPbI_3$ revealed that the effect of humidity was minimal in case of single crystals.[48] Furthermore, ion migration occurs more freely along grain boundaries which can pose stability issues for the long term usage of PSCs.[49] After realizing one-step spin coating was not adequate for achieving pinhole-free coverage of the substrate, techniques such as two-step sequential deposition,[50] anti-solvent assisted spin coating,[11] the lewis acid-base adduct approach,[46] vapor assisted solution processing,[13] and co-evaporation[12] were explored. While these alternative techniques were able to produce pin-hole free and full coverage films, there was still scope for further improvement in terms of grain size, crystallinity, homogeneity, and scalability of the perovskite layer to enhance the PSC performance. It should be noted that anti-solvent assisted spin coating is still a widely used technique and frequently used in conjugation with other techniques for further improvement of the perovskite layer.

Several interesting techniques have emerged to achieve high quality large grain perovskite films such as hot-casting, additive engineering, non-wetting-assisted crystallization, meniscus-assisted solution printing, intermolecular exchange method and polymer-templated nucleation (**Figure 3**). These techniques not only produce micrometer to millimeter grains but also, in some cases, are capable of producing monolayers of single-crystalline grains.[51] In this section we

discuss some highly efficient PSCs based on large grain polycrystalline perovskite layers and the relevant techniques of deposition.

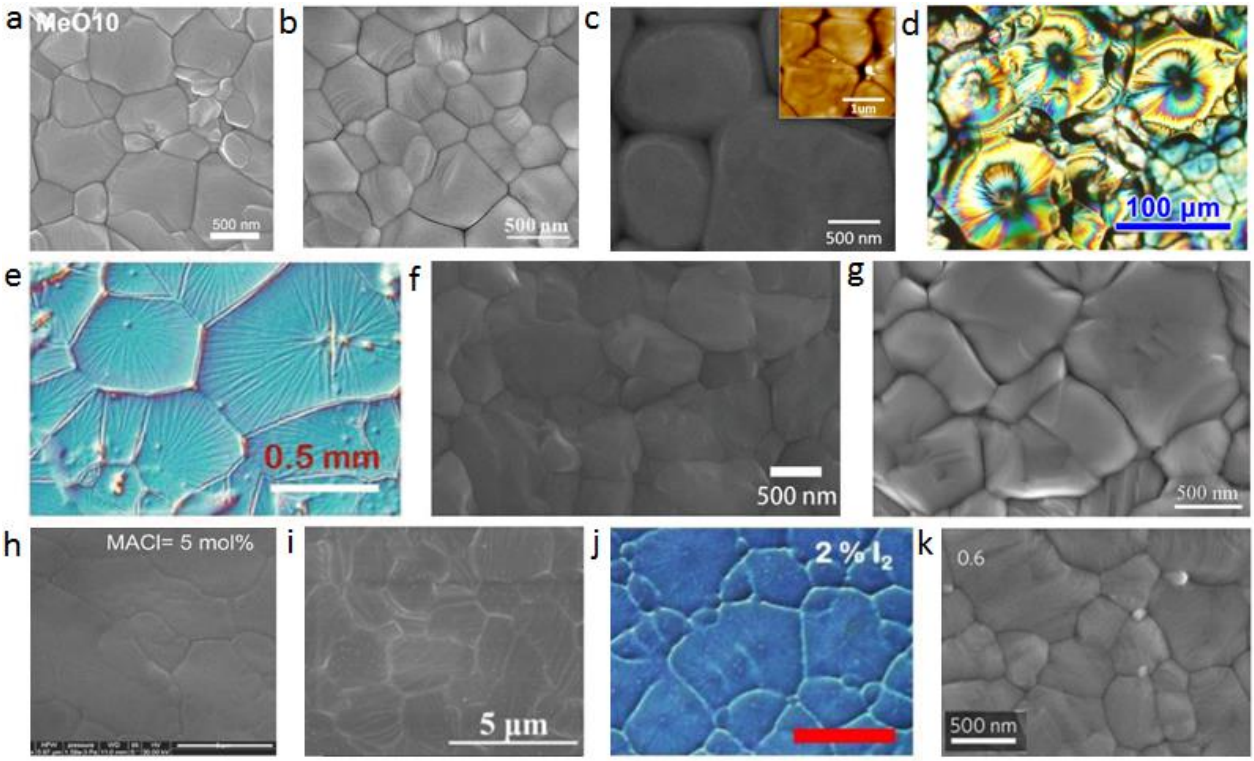

Figure 3. SEM and optical images of polycrystalline perovskite films obtained by various emerging strategies. a) Dual additive-mediated crystallization. Reproduced with permission.[52] Copyright 2019, American Chemical Society. b) Gas-assisted solution processing. Reproduced with permission.[51] Copyright 2014, Elsevier. c) Merged annealing method. Reproduced with permission.[53] Copyright 2017, American Chemical Society. d) Precursor solution from perovskite single crystal powder. Reproduced with permission.[54] Copyright 2016, American Chemical Society. e) Hot-casting technique. Reproduced with permission.[38] Copyright 2015, American Association for the Advancement of Science. f) Intermolecular exchange method. Reproduced with permission.[55] Copyright 2015, American Association for the Advancement of Science. g) Vacuum flash–assisted solution processing. Reproduced with permission.[56] Copyright 2016, American Association for the Advancement of Science. h) Doctor blading with 5 mol% MACl additive, scale: 2 µm. Reproduced with permission.[57] Copyright 2017, Wiley-VCH. i) Temperature controlled direct contact intercalation process. Reproduced with permission.[58] Copyright 2016, Royal Society of Chemistry. j) Host-casting with I_2 addition, scale: 50 µm. Reproduced with permission.[59] Copyright 2015, American Chemical Society. k) Polymer-templated nucleation. Reproduced with permission.[60] Copyright 2016, Nature Publishing Group.

2.1. Hot-Casting

In the hot-casting method proposed by Mohite et al., a heated perovskite precursor solution (PbI_2, MACl, 70 °C) is spin-coated onto a substrate held at an elevated temperature (180 °C).[38] Using this technique pinhole-free perovskite films were achieved with millimeter-scale crystalline grains (**Figure 3**e). Grain sizes of 1-2 mm were obtained with this method, compared to 1-2 µm using conventional spin coating and post annealing process. These grains have a leaf-like structure growing from a central nucleation site towards the edge. Polarized light images of the hot-casted films indicate a single-crystalline nature of the grains. However, scanning electron microscope (SEM) images exhibit some unusual features: for instance, the top surface of the film shows grain boundary-type features, but in the cross-sectional SEM image, such features are absent. While it is not clear what causes the top layer to be different than the bulk, it was proposed that solvent evaporation during the spin coating process may be a probable cause. Advanced techniques such as electron backscatter diffraction (EBSD) and point focus XRD techniques can help in unambiguously proving the single-crystalline nature of such grains. It should be noted that morphological grains (as identified by SEM/optical images) are not representative of true crystallographic grain size.[61] Planar PSCs based on hot-casted films resulted in an efficiency of 18% with organic charge transport layers. It was found that in hot-casted $MAPbI_3$ films, there was some amount of $MAPbCl_3$ present as a result of Cl containing precursors. In a subsequent work, I_2 was added as additive to control the chemical composition of the hot-casted perovskite films.[59] Adding I_2 reduces the quantity of $MAPbCl_3$ and promotes the formation of $MAPbI_3$. Interestingly, the average grain size reduces from 28 to 11 µm upon the addition of 10% I_2 addition indicating presence of $MAPbCl_3$ also plays a role in determining the grain size. A peak efficiency of 15.58% was achieved for the perovskite film with 2% I_2 added

(**Figure 3**j) in contrast to 9.83% for films without I_2 owing to the promotion of the preferred $MAPbI_3$ phase.

The rapid crystallization of perovskite films using the hot-casting method makes it a promising technique for large scale fabrication. Marks et al. fabricated large-area PSCs to test the feasibility of the technique:[62] PbI_2 and MAI with various amounts of a Cl-containing precursor were chosen to optimize the device efficiency. They fabricated planar PSCs by hot-casting technique with NiO_x as HTL and PCBM as ETL. Efficiencies of 18.2%, 15.4%, and 12% were achieved for devices with an active area of 0.09 cm^2, 1 cm^2, and 5 x 5 cm eight-cell module, respectively. The encapsulated module exhibited high stability for 1500 hours while maintaining >90% efficiency under ambient conditions. Building on hot-casting, a hot dip-coating technique was developed whereby a heated substrate is dipped in a hot precursor solution and removed quickly. An efficiency of 12.4% was recorded for PSCs by hot-dipping technique. Dip-coating is an industrially viable technique with compatibility with existing technologies, aside from issues arising from solvent toxicity. There is a possibility of improving the efficiency to even high values if thinner perovskite films can be obtained by further modification of the hot dip-coating technique.

2.2. Additive Engineering

Additive engineering of perovskites has emerged as a potential technique to modify the morphological and electronic properties. One recent report yielding a very high efficiency of 23.48% for PSCs was achieved by adding MACl in $FAPbI_3$. The MACl addition resulted in a 6 times increase in grain size, 33 times increase in phase crystallinity, and 4.3 times improvement in photoluminescence lifetime.[63] The additives can be broadly classified into three categories: First, those which improve the perovskite's morphology or structural properties. Second, those which enhance electronic properties by trap passivation and improving charge transport. Third,

additives which have a bifunctional character which improve the morphology as well as electronic characteristics of perovskites. A number of additives with diverse properties have been explored to improve the performance of PSCs.

In one early work, Adachi et al. added photochemically active additive benzoquinone (BQ) to the $MAPbI_3$ precursor solution.[64] Molecular interactions between BQ and MAI resulted in retardation of crystallization, leading to formation of uniform compact perovskite films with large grains and better crystallinity. An efficiency of 15.6% was achieved for planar PSCs with BQ additive compared to 10.7% for devices without the additive. In another work, Liu et al. mixed N,1-diiodoformamidine (DIFA) as an additive in $FA_{0.85}MA_{0.15}PbI_3$ precursor solution resulting in smooth films with μm size grains.[65] In addition, optimized concentration of 2% DIFA reduces the trap density and prolongs carrier lifetime. PSCs based on DIFA additive resulted in an efficiency of 21.22% compared to 19.07% for pristine devices.

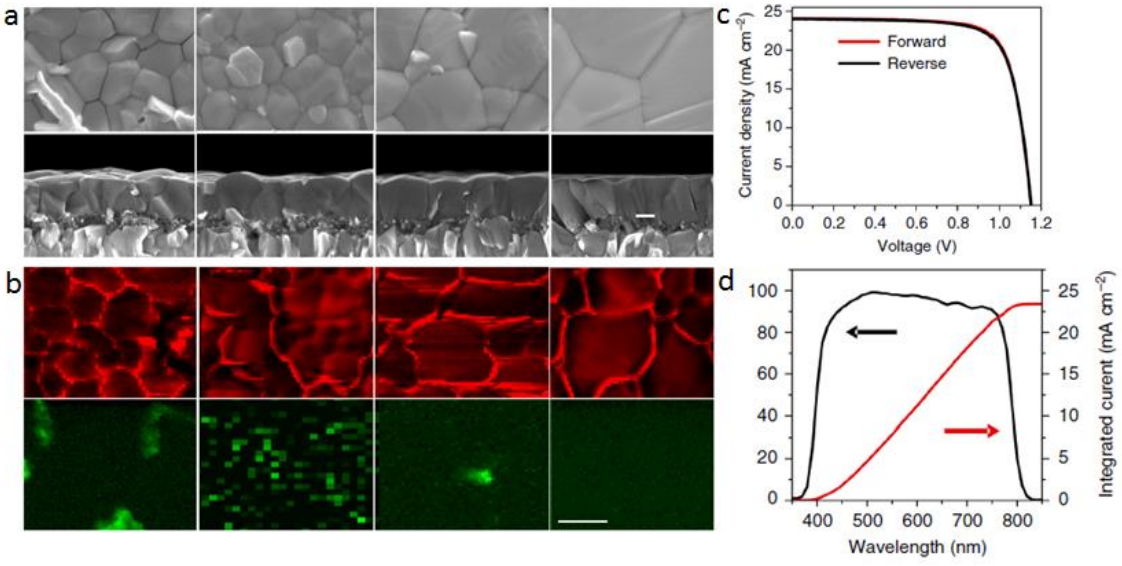

Figure 4. Structural characterization of modulated perovskite films. a) Plane-view (top) and cross-sectional (bottom) SEM images of the pristine (control) and modulator-containing (N, S, and SN) perovskite films deposited on the mesoporous TiO_2/compact-TiO_2/FTO. Scale bar represents 200 nm. b) Cathodoluminescence (CL) mapping of the pristine (control) and additive-containing (N, S, and SN) perovskite films deposited on the ITO (1 mm) glass substrates. The

spatial distribution of green and red light emission, recorded from 530 to 590 nm and from 700 to 800 nm, respectively, reveals the microscopic distribution of PbI_2 phase in the perovskite films. Scale bar represents 1 μm. c) J–V curves of the champion cell containing SN recorded in reverse (from V_{OC} to J_{SC}) and forward (from J_{SC} to V_{OC}) scanning directions under standard AM 1.5G solar radiation. d) The corresponding IPCE spectrum (black curve) with the projected photocurrent (red curve) derived from integrating the IPCE over the standard AM 1.5G spectral emission. Reproduced with permission.[66] Copyright 2018, Nature Publishing Group.

Dual additive approaches have also been explored for PSCs, where two additives are added to improve the perovskite layer. Han et al. added ionic-liquid additive of methylammonium acetate (MAAc) and a molecular additive of thio-semicarbazide (TSC) to the $MAPbI_3$ precursor solution.[67] The addition of MAAc results in highly uniform and fully-covered perovskite films, while the addition of a small amount of TSC leads to grain size enhancement. A certified efficiency of 19.19% was achieved for planar PSCs with an aperture area of 1 cm^2. Furthermore, the PSCs maintained stability of over 80% of initial efficiency after 500 hours of thermal aging at 85 °C. Clearly, the dual additive approach enhances both the efficiency, as well as stability of PSCs.

In a more recent work, Gratzel and coworkers explored three molecular modulators namely including thiol-based 5-(methylthio)-1H-tetrazole (S), ammonium-based anilinium iodide (N), and bifunctional 3-(5-mercapto-1H-tetrazol-1-yl) benzenaminiumiodide (SN) to improve the performance of PSCs as well as to understand how each modulator modifies the $FA_{0.9}Cs_{0.1}PbI_3$ perovskite layer.[66] It was found that thiol-based modulator S has ability to increase the grain size and passivate unsaturated Pb(II) ions on the surface while the ammonium-based modulator N alleviates lattice defects. The modulator SN combines the beneficial characteristics of both S and N modulators resulting in simultaneous improvement of grain size and crystallinity, as well as reducing nonradiative recombination defect centers in the perovskite layer. The grain boundary area, in the case of modulator SN, was significantly reduced in contrast to control, S,

and N samples. Cathodoluminescence mapping and XRD of the films indicated the presence of residual PbI_2 in the control, S, and N samples, which was otherwise absent (or amorphized) in SN samples. The pronounced effect of modulator SN on the perovskites can be observed in terms of enlarged grain size as well the absence of PbI_2 phase. It was proposed that the molecular modulation of the perovskite layer in the presence of SN can take place through hydrogen bonding of the donor groups ($–NH^{3+}$, –NH) to the perovskite surface and interaction with the Pb^{2+} ions via thione (C=S) coordination. As a result of their enhanced morphological, structural, and electronic properties, PSCs based on a SN modulator exhibited an efficiency of 20.9% using mesoporous TiO_2 architecture (**Figure 4**). Exceptional stability of 1000 hours was also recorded for SN-based devices, with full solar light soaking of unsealed devices at 60 °C under Ar gas.

There are many more additives which have been explored either to enhance the grain size, crystallinity, or efficiency of PSCs. Lead Thiocyanate ($Pb(SCN)_2$) was found to increase the perovskite grain size and fill factor of PSCs while reducing the hysteresis behavior.[68] Ammonium benzenesulfonate acts as a bifunctional additive resulting in improved perovskite film quality and reduced defect densities.[69] Interestingly, even additives, as simple as acetonitrile in the precursor solution was found to a marked effect on the perovskite film quality.[70] More examples of additives with PSC performance details are shown in **Table 1**. Additive engineering has proven to be a promising approach for perovskite film modification as it does not require any additional fabrication step or special instrumentation.

2.3. Non-Wetting Behavior and Surface Modification

The surface beneath the perovskite layer has a key influence on the morphology and the quality of the interface. Initially, significant efforts were dedicated to modify the surfaces of charge transport layers particularly, for oxide ETLs termed as “interface engineering”. The

advantages of such modifications were many-fold: Improved perovskite morphology, a better electronic interface between the charge transport layer and perovskite, and trap passivation.[71-75] Later, it was found that the wetting properties of charge transport layers play a significant role and tuning their surface properties can result in deposition of high-quality perovskite films.

In an important finding, Huang et al. demonstrated that the hydrophobic nature of different polymeric HTL layers can be utilized to grow large grain perovskite layers.[76] The hydrophobicity increases the nucleus spacing by suppressing heterogeneous nucleation, thereby reducing the number of grain boundaries. For comparison, films were grown on a number of wetting and non-wetting polymer layers such as polyvinyl alcohol (PVA), poly(3,4-ethylenedioxythiophene) polystyrene sulfonate (PEDOT:PSS), crosslinked N4,N4′-bis(4-(6-((3-ethyloxetan-3-yl)methoxy)hexyl)phenyl)-N4,N4′-diphenylbiphenyl-4,4′-diamine (c-OTPD), poly(bis(4-phenyl)(2,4,6-trimethylphenyl)amine) (PTAA) and poly (N-9′-heptadecanyl-2,7-carbazole-alt-5,5-(4′,7′-di-2-thienyl-2′,1′,3′-benzothiadiazole)) (PCDTBT). Wetting polymer layers of PVA and PEDOT:PSS lead to perovskite films with small grains in contrast to non-wetting layers of c-OTPD, PTAA, and PCDTBT. In case of PCDTBT, grains as large as 5 μm were observed, but the perovskite layer was not continuous due to very high hydrophobicity. Planar PSCs based on c-OTPD and PTAA HTL exhibited efficiencies of 17.8% and 18.1%, respectively. The $MAPbI_3$ layer was fabricated by interdiffusion method where first PbI_2 layer is coated, and then the MAI is coated on the top.[77] Annealing this bilayer structure at 110 °C results in smooth perovskite layers. Enlarged grain size in case of hydrophobic HTLs also result into low trap densities as well as improved HTL/perovskite interface. In another work, PSCs based on hydrophobic PTAA HTL resulted in enlarged grain as well as phase stabilization of $MAPbBr_xI_{3-x}$ grains fabricated by interdiffusion method resulting in improved efficiency of

16.6%.[78] Bigger grains and better crystallinity of the perovskite layer was the key to preserve the homogeneous phase under illumination.

The non-wetting character of HTL layer is able to generate large grain films by interdiffusion method as discussed above, but due to high hydrophobicity, it is difficult to achieve full coverage by one-step spin coating. While hydrophobicity is important, very high hydrophobicity can make it difficult to deposit reproducible perovskite films by one-step spin-coating. To tackle this issue, Gong et al. introduced a hydrophilic group (C–O & C=O) grafted buffer layer on hydrophobic PTAA HTL to decrease the surface potential and surface tension.[79] The treated PTAA resulted in smooth, dense, pin-hole free $(Cs_{0.05}(FA_{0.85}MA_{0.85})_{0.95}Pb(I_{0.85}Br_{0.15})_3$ films by anti-solvent assisted spin coating. Planar PSCs based on treated PTAA exhibited a high efficiency of 20.75% with high reproducibility and enhanced humidity stability.

Though non-wetting behavior of PTAA and its surface modification are successful in generating highly efficient PSCs with small active areas, it is important to test if these techniques are scalable. In a recent work, it was shown addition of a small amount of surfactant in perovskite precursor solution can enable large grain uniform coating of perovskites on hydrophobic PTAA in air for PSC modules.[80] A number of surfactants were explored, including L-α-phosphatidylcholine (LP), polyethylene glycol sorbitan monostearate (Tween 60), sodium dodecyl sulfate (SDS) and didodecyldimethylammonium bromide (DDAB), which are amphoteric, non-ionic, anionic and cationic surfactants, respectively. Surfactant-added films exhibited uniform thickness and continuous morphology in contrast to the control sample (**Figure 5**). Surfactant LP was selected for further optimization as LP has been shown previously to passivate traps in perovskites[81] and exhibited higher efficiencies than other surfactants. LP-containing $MAPbI_3$ ink was blade coated on PTAA layer for fabrication of PSCs.

Compared to the control sample, the surfactant pins the contact line to the substrate resulting in uniform coverage of perovskite films suggesting the successful modification of the ink/PTAA interface and improved affinity between them. Maximum efficiency of 20.3% was recorded for devices with architecture ITO/PTAA/$MAPbI_3$/C60/BCP/Cu with an active area of 0.075 cm^2. Further to prove the scalability of the technique, surfactant-assisted blade coating was employed to fabricate modules resulting in impressive efficiencies of 15.3% and 14.6% achieved for modules with an area of 33 cm^2 and 57.2 cm^2, respectively.

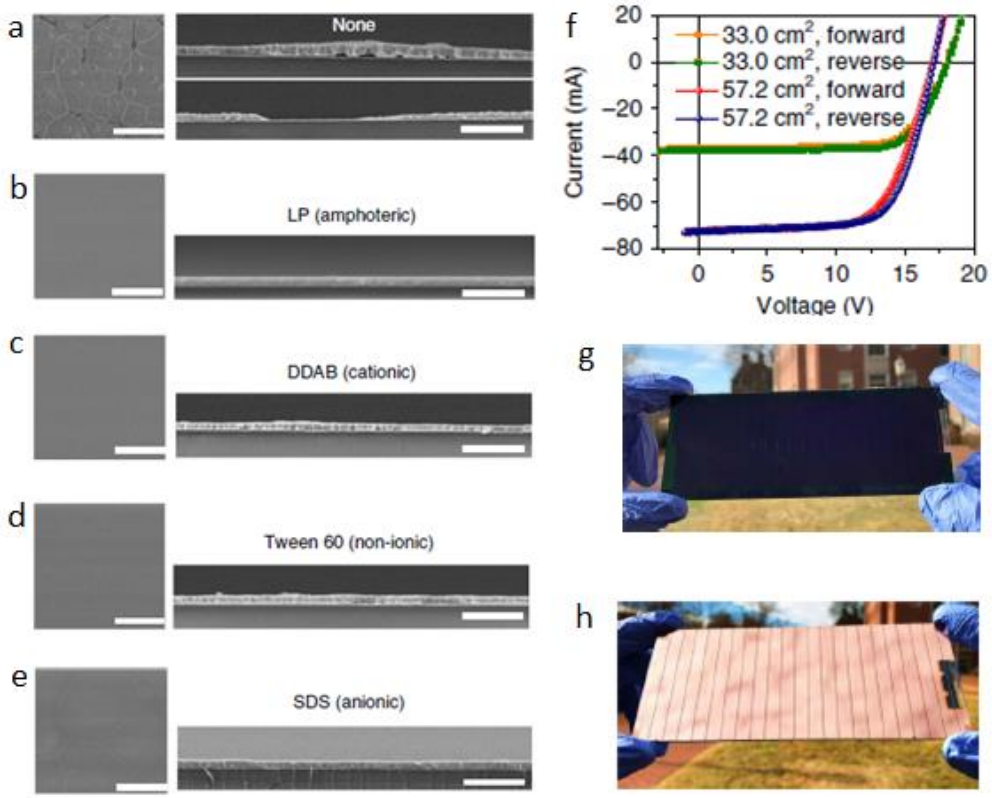

Figure 5. a-e) Plane view and cross-sectional SEM images of bladecoated perovskite films without surfactant and with LP, DDAB, Tween 60 and SDS, respectively. Scale bars for plane view and cross-sectional SEM images are 50 μm and 5 μm, respectively. f), *I–V* scanning curves of modules with aperture areas of 33.0 cm^2 and 57.2 cm^2. Photographic image of a perovskite solar module viewed from the g) glass side and h) top electrode side. Reproduced with permission.[80] Copyright 2018, Nature Publishing Group.

2.4. PSCs by Blade coating

Doctor blading of the perovskite layer is gaining momentum as a suitable technique for large scale fabrication. Also, the amount of precursor solution needed for film deposition is lower than other techniques such as spin coating, reducing material wastage.[82] In one work, the importance of composition engineering of perovskites was recognized for achieving high-quality blade coated films. Huang et al. blade coated $MA_{0.6}FA_{0.38}Cs_{0.02}PbI_{2.975}Br_{0.025}$ films with large grains leading to stabilized efficiency of 19.3% for planar PSCs.[57] The addition of a small amount of Cs^+ and Br^- to a $(MAPbI_3)_{0.6}(FAPbI_3)_{0.4}$ mixed precursor solution enabled improved phase purity and allowed for doctor blading of $MA_{0.6}FA_{0.38}Cs_{0.02}PbI_{2.975}Br_{0.025}$ at 120 °C. In addition, Methylammonium chloride (MACl) was added as an additive to further improve the film coverage and grain size.; an example of combinatorial approach (mixed perovskite, blade coating, and additive engineering) for depositing high-quality large grain perovskite films for high performance PSCs. The addition of 5 mol% MACl resulted in µm size grains with 100% film coverage. Interestingly, blade coating is also capable of producing vividly colorful-appearing PSCs under specific conditions. In one early work, doctor blading of $MAPbI_3$ precursor solution produced large 20-100 µm size domains with a concentric ring photonics structure resulting in colorful PSCs with 12.2% efficiency.[83] Such colorful PSCs might be interesting for building-integrated photovoltaic applications in the future.

Recently, a modified version of blade coating termed “meniscus-assisted solution printing” (MASP) was demonstrated to achieve large grain $FA_{0.85}MA_{0.15}PbI_{2.55}Br_{0.45}$ films with preferred orientation.[84] In this technique, the solvent evaporation is driven by the meniscus effect in contrast to high temperature as in case of blade coating. In MASP, the solvent evaporation is faster near the edge of the meniscus ink resulting in transport of perovskite solutes towards the

meniscus front, creating a supersaturated phase (**Figure 6**). Tracking of perovskite film growth by optical microscopy revealed that small perovskite grains appeared initially in front of the meniscus ink which, then underwent 2D growth into large island and eventually merge with other nearby grains. This technique produced densely packed grains with size of 20-80 µm, with no voids at grain boundaries. The thickness of the perovskite layer in a wide range (~600 nm - 2.7 µm) can be tuned by the concentration of the precursor solution. An efficiency of 20.05% was achieved in a planar architecture PSC with TiO_2 and PTAA as ETL and HTL, respectively. Furthermore, an efficiency of 18.02% was recorded for a large area PSC of 0.98 cm^2. There is a possibility of extending the MASP technique to other solution-processed semiconductors such as those found in organic photovoltaics and light emitting diodes.

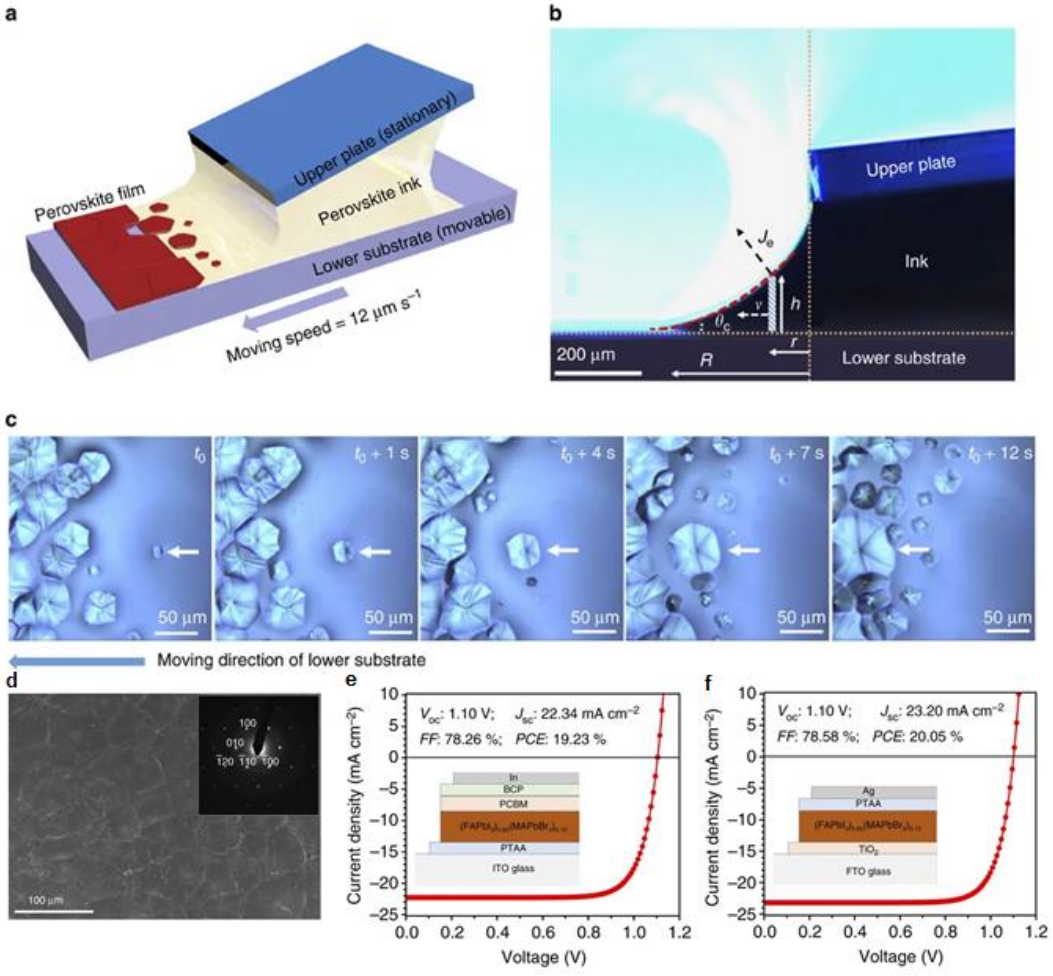

Figure 6. Meniscus-assisted solution printing of $FA_{0.85}MA_{0.15}PbI_{2.55}Br_{0.45}$ perovskite crystal films. a) Schematic illustration of the meniscus-assisted solution printing (MASP) of large-grained perovskite films. b) Optical micrograph of the side-view meniscus ink confined between a lower flat, movable substrate and an upper stationary plate. c) Optical micrograph of the microstructural evolution of perovskite grain as a function of time. d) SEM image of the perovskite film crafted by MASP. A representative selected area electron diffraction (SAED) of the perovskite film is shown as an inset. e) Current density–voltage (J–V) characteristic of the inverted planar perovskite solar cell. The device architecture is shown as an inset. f) J–V characteristic of the standard planar perovskite solar cell. The device architectures are shown as insets. Reproduced with permission.[84] Copyright 2017, Nature Publishing Group.

In addition to the above discussed approaches, there are several other techniques for achieving large grain uniform perovskite films including polymer template assisted crystallization,[60] electrohydrodynamically assisted deposition,[85] direction contact and intercalation process,[58] intramolecular exchange[55] and so on. More examples of emerging techniques with PSC performance details are shown in **Table 1**.

Table 1. Some representative works on state-of-the art PSCs with fabrication and performance details.

Perovskite	Deposition Method	Additive (A)/ Technique (T)	Device structure	Best η (%)	Year	Ref
$MAPbI_3$	Spin coating	A: $Pb(SCN)_2$	planar	18.42	2016	[68]
$MAPbI_3$	Interdiffusion	A: Acetonitrile	planar	19.70	2016	[70]
$MAPbI_3$	Spin coating	T: Merged annealing	planar	18.27	2017	[53]
$MAPbI_3$	Hot-casting	A: $PbCl_2$, MACl	planar	18.20	2017	[62]
$MAPbI_3$	Spin coating	A: MAAc,[a] TSC[b]	planar	19.19	2017	[67]
$MAPbI_3$	Anti-solvent assisted spin coating	A:Thiourea	meso	19.80	2018	[86]
$MAPbI_3$	Blade coating	A: L-α - Phosphatidylcholine	planar	20.30	2018	[80]
$MAPbI_3$	Anti-solvent assisted spin	A: DMSO,[c] methoxyammonium	meso	19.71	2019	[52]

	coating	salt				
$MAPbI_3$	Anti-solvent assisted spin coating	T: micro-contact print	planar	20.08	2019	[16]
$FAPbI_3$	Spin coating	T: Intramolecular exchange	meso	20.20	2015	[55]
$FAPbI_3$	Anti-solvent assisted spin coating	A: MACl	meso	24.02	2019	[63]
$(FAI)_{0.81}(PbI_2)_{0.85}(MAPbBr_3)_{0.15}$	Spin coating	T: Polymer template assisted crystallization	meso	21.6	2016	[60]
$MA_{0.6}FA_{0.38}Cs_{0.02}PbI_{2.975}Br_{0.025}$	Blade coating	A: MACl	Planar	19.3	2017	[57]
$FA_{0.85}MA_{0.15}PbI_{2.55}Br_{0.45}$	Blade coating	T: Meniscus-assisted solution printing	planar	20.05	2017	[84]
$FA_{0.9}Cs_{0.1}PbI_3$	Spin coating	A: SN[d] T: vacuum-flash	meso	20.9	2018	[66]
$FA_{0.85}MA_{0.15}PbI_{2.55}Br_{0.45}$	Anti-solvent assisted spin coating	A: Ammonium benzenesulfonate	meso	20.62	2019	[69]
$FA_{0.85}MA_{0.15}PbI_3$	Spin coating	A: DIFA[e]	planar	21.22	2019	[65]

[a)]MAAc: methylammonium acetate; [b)]TSC: thio-semicarbazide; [c)]DMSO: Dimethyl sulfoxide; [d)]SN: 3-(5-mercapto-1H-tetrazol-1-yl) benzenaminium iodide; [e)]DIFA: N,1-diiodoformamidine

It is evident from the above discussions that significant efforts have been dedicated to improving the quality of the perovskite layer for efficient PSCs in terms of increasing the grain size. While millimeter-scale grains have been achieved for polycrystalline PSCs, the negative effects of grain boundaries on the performance and stability of PSCs remain. In terms of trap density, polycrystalline films have orders of magnitude higher trap densities compared to single crystals.[87] In addition, recent works show that there has been a momentous simplification of techniques used for growing large single crystals of halide perovskites for device applications. This leads to the tantalizing proposition that fabricating grain boundary-free, single crystal PSCs might be the next step in development of robust PSCs devices. In the next section, we discuss the

developments pertaining to SC-PSCs and the related opportunities and challenges presented by such SC devices.

3. Perovskite Single Crystals: Growth Techniques and SC-PSCs

Perovskite materials have a long history before the reemergence of their hybrid form in 2009. The first halide perovskites were reported in 1890s and were all-inorganic materials based on Cs.[88] The first crystallographic details of the halide-containing perovskites was reported in 1958.[89] The 3D hybrid perovskites were synthesized by replacing Cs with MA in 1978.[90-91] Sn-based 2D perovskites were also explored as transistors materials in the 1990s.[92] The sizes of these early single crystals were very small and not suitable for device fabrication. They were mainly used in X-ray diffraction studies to obtain crystallographic information. In addition to the conventional methods of growing single crystals, various modified and new crystal growth techniques have been explored for growing large hybrid perovskite single crystals (**Figure 7**). These crystal growth techniques can be broadly classified into two categories: Bulk crystal techniques and thin crystal techniques. While bulk crystals are comparatively easier to grow and larger in size, thin crystals are more suitable for device applications. Thin crystals can also be grown on different substrates, which provide mechanical support as well as making their handling easier.

Among the various methods of free-standing bulk crystal growth, perovskite single crystals with size 2-10 mm have been reported with methods including anti-solvent vapor assisted crystallization,[4] slow solvent evaporation,[93] low-temperature gradient crystallization[94] and inverse temperature crystallization (ITC).[95] Interestingly, with seed-induced crystallization, single crystals larger than 50 mm have been grown.[96] In anti-solvent vapor assisted crystallization technique, the perovskite precursor solution is surrounded by a solvent in which

hybrid perovskite precursors are insoluble.[4] The slow diffusion of the anti-solvent into the precursor solution leads to precipitation and growth of the crystal over time. The fastest perovskite crystal growth technique is ITC. In one work, bulk crystals of $MAPbI_3$ and $MAPbBr_3$ were grown within minutes employing ITC.[97] Despite the rapid growth process, these crystals had optical and transport properties equal to those grown by slower processes such as solvent cooling.

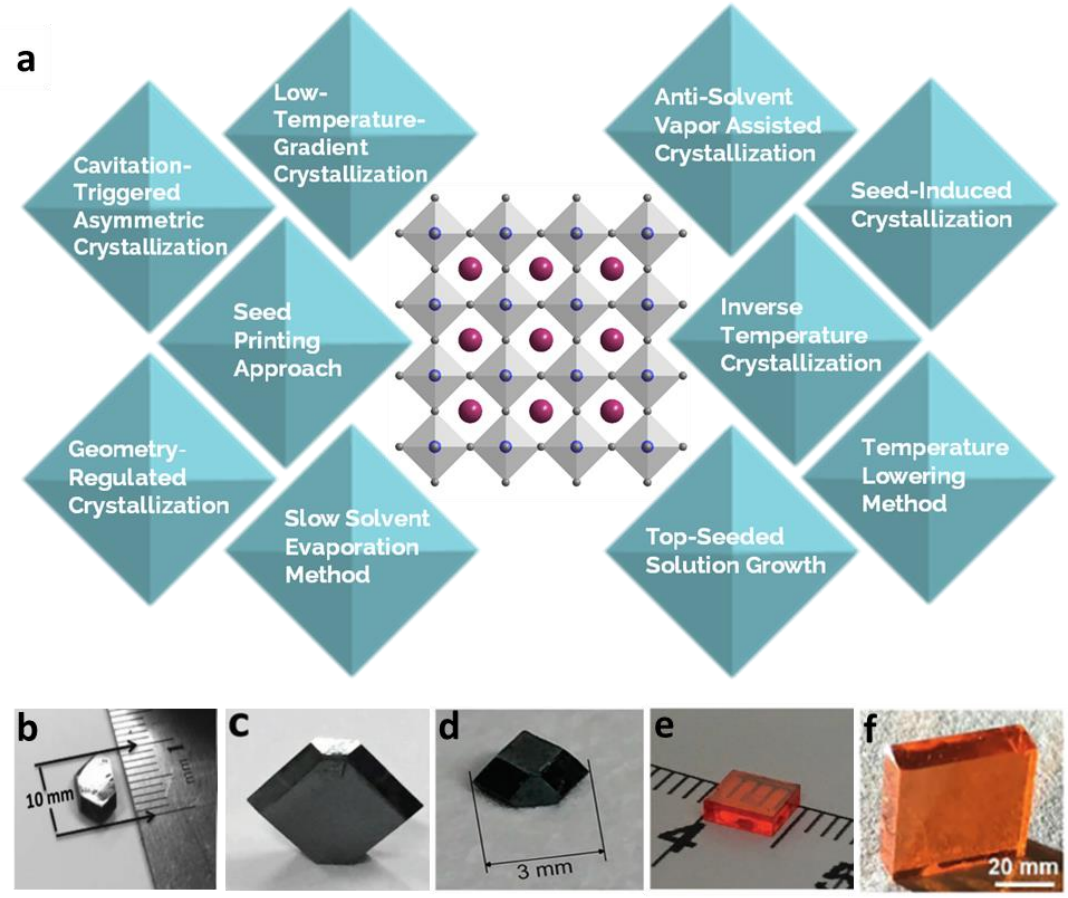

Figure 7. a) Various methods of growing hybrid perovskite single crystals.[4,7,93-96,98-101] b) $MAPbI_3$ grown by top-seeded solution growth. Reproduced with permission.[7] Copyright 2014, American Association for the Advancement of Science. c) $MAPbI_3$ grown by geometry regulated crystallization. Reproduced with permission.[102] Copyright 2018, Wiley-VCH. d) $FAPbI_3$ grown by ITC. e) $FAPbBr_3$ grown by ITC. Reproduced with permission.[103] Copyright 2015, Royal Society of Chemistry. f) $MAPbBr_3$ grown by low-temperature gradient crystallization. Reproduced with permission.[94] Copyright 2019, Elsevier.

In the case of thin single crystals, more specific crystallization techniques have been developed, such as cavitation-triggered asymmetric crystallization, space-limited/geometry-regulated crystallization, and surface tension-controlled ITC.[98,100,104] The most common technique to grow thin SC-perovskite crystals is space-limited crystallization. In this technique, two substrates are clamped together with a cavity in-between. The thickness of the perovskite crystal can be controlled by adjusting the gap between the two substrates. The clamped substrates are submerged in a perovskite precursor solution and heated. Capillary action and heat gradient leads to the formation of thin single crystals in the cavity between substrates. We will discuss the crystallization techniques relevant to the SC-PSCs in the next section. Readers are encouraged to refer to recent reviews on hybrid perovskite single crystal growth techniques for further details.[105-106]

The best-performing PSCs reported in the literature to date are typically prepared with the help of suitable metal-oxide charge transporters and engineered interfaces.[29,35,55,107] However, there has also been research on PSCs that do not contain either hole or electron transport layers. The argument underlying such a drastic simplification of the device architecture is that hybrid perovskites are already sufficiently effective charge transporters by themselves. In one representative work by Shi et al., an HTM-free PSC with a structure of TiO_2/$MAPbI_3$/Au was fabricated and shown to exhibit a power conversion efficiency of 10.4%.[108] A similar efficiency was achieved by Jin and colleagues using a device structure of ZnO/$MAPbI_3$/graphite/carbon black.[109] Inspired by earlier works, Liu et al. fabricated electron transfer material (ETM)-free solar cells via the sequential deposition of $MAPbI_3$, achieving an efficiency of 13%.[110] A similar work was reported by Ke et al. in which $MAPbI_{3-x}Cl_x$ was used as the perovskite absorber, resulting in an efficiency of 14%.[111] In this work, ultraviolet (UV)–ozone

moditication of the FTO substrate's work function was crucial in achieving high performance, indicating the importance of the FTO/perovskite interface. Similar to these polycrystalline PSCs, SC-PSCs have been fabricated with and without charge transport layers. In this section, we summarize the SC-PSCs with vertical and lateral architectures and the effect of charge transport layer on performance. In addition, the crystallization techniques developed to grow the perovskite single crystals for SC-PSCs are also discussed.

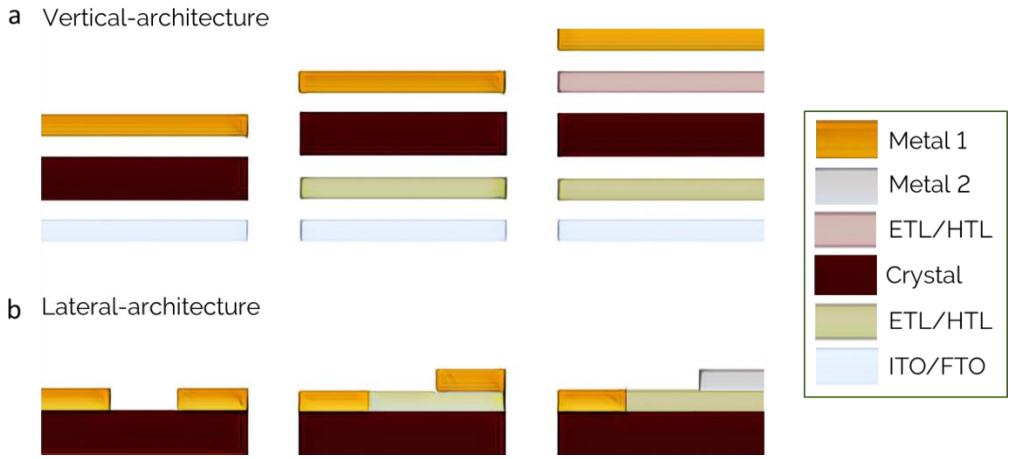

Figure 8. Various architectures of SC-PSCs.

3.1. Vertical-Structure SC-PSCs

There are three main types of vertical-structure SC-PSCs as shown in **Figure 8a**: Devices with no charge transport layers are directly grown on ITO or FTO-coated glass substrates, with Au thermally evaporated as the top contact. For second type of devices, a single crystal is grown atop the charge transport layer (ETL/HTL) coated substrate (ITO/FTO). These devices only contain one charge transport layer at the buried interface, with Au directly deposited on top of the crystal. The third type of device has both ETL and HTL on either side of the perovskite. Depending on the charge transport layers, it can be *p-i-n* or *n-i-p* structure.

In one early work, Li et al. fabricated SC $MAPbI_3$ arrays by a droplet-pinned crystallization technique.[112] To form the SC arrays, precursor solution is dropped on the substrate, and a

silicon wafer is placed on the top of the precursor droplet to pin it to the substrate. Upon heating, SC arrays with width in tens of microns grow along the receding direction of the droplet as a result of solvent evaporation. For fabricating the SC-PSC, arrays were grown on top of PEDOT:PSS-coated ITO substrates. PCBM/ZnO was deposited as the ETL layer, and finally Al as the top contact electrode. The resulting SC-PSC exhibited an efficiency of 1.73%, which is significantly lower than polycrystalline PSCs. The low performance of the SC-PSC can be attributed to the direct contact between the ETL and HTL layer as a result of incomplete coverage of the $MAPbI_3$ arrays. In the first of such works, Liu et al. reported SC-PSCs based on $MAPbI_3$ wafers by slicing large single crystals.[113] While the performance of the SC-PSC was modest (~ 4% PCE), it offers an interesting route of growing very large perovskite single crystals and obtaining wafers.

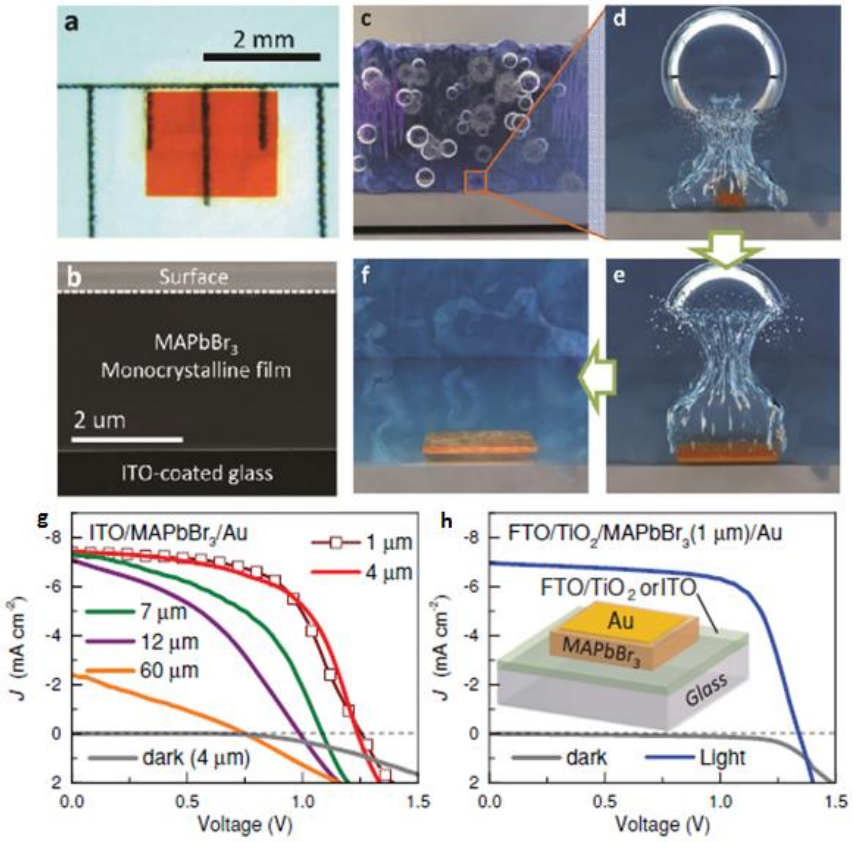

Figure 9. a) Optical image of the monocrystalline film. b) Cross-section SEM image of a freshly cut monocrystalline film. c–f) Illustrations of the CTAC mechanism on a microscopic scale. c) An ultrasonic pulse induces cavitation in the perovskite solution. d–f) Collapse of the cavitation bubble at the neighborhood of a substrate is asymmetric and results in a high-speed jet toward the substrate, which is the origin of preferential lateral crystallization at the initial stage. Dark and illuminated J–V curves. g) ITO-based SC-PSC. h) FTO/TiO_2-based SC-PSC. Reproduced with permission.[98] Copyright 2016, Wiley-VCH.

Bakr et al. developed an interesting crystallization technique with the aid of ultrasonic pulsation for growing thin SC $MAPbBr_3$ directly on substrates (**Figure 9**).[98] This technique is based on anti-solvent vapor crystallization and termed as cavitation-triggered asymmetrical crystallization (CTAC). A short ultrasonic pulse (<1 s) is applied to the precursor solution when the supersaturation reached a low level due to anti-solvent diffusion. Ultrasonication releases an intense burst of energy, accompanied by a cavitation process that leads to nucleation by overcoming the nucleation energy barrier. These cavitation bubbles collapse near the substrate, which is asymmetric in nature and results in a high-speed jet towards the substrate which is the origin of the preferential lateral growth in the initial stage of crystal growth. An efficiency of 5.4% was recorded with the SC-PSC architecture ITO/$MAPbBr_3$/Au and 6.5% for FTO/TiO_2/$MAPbBr_3$/Au. The crystal thickness in both cases was 1 µm. A high open circuit voltage (V_{oc}) of 1.4 V was achieved in case of devices with TiO_2 ETL. Furthermore, the CTAC method can be extended to a range of substrates including ITO, FTO, silicon wafers, and metal coated silicon. In another work, Kuang et al. using space-limited ITC, grew SC-$MAPbBr_3$ and achieved an efficiency of 7.11%.[114] To fabricate SC-PSC, $MAPbBr_3$ were grown on TiO_2 coated FTO substrates and Spiro-OMeTAD was used as the HTL. SC-PSCs exhibited impressive stability, maintaining 93% of initial efficiency after aging for 1000 hours in dry air without encapsulation, further lending credibility to the hypothesis that grain boundaries are initiation sites for device degradation.

Space-limited crystallization of hybrid perovskites has also attracted significant attention, particularly to grow thin crystals. This technique can be employed to a wide variety of hybrid perovskites and offers a large degree of tunability. Li et al. succeeded in growing sub-square, centimeter-scale thin sheets of $MAPbBr_3$ using space-limited crystallization.[115] Furthermore, the crystallization technique can be adjusted to grow centimeter-scale $MAPbBr_3$ wires by manipulating the growth temperature. The growth behavior of $MAPbBr_3$ has a strong dependence on temperature. Rectangular $MAPbBr_3$ sheets were obtained at higher temperatures due to solubility-dominated nucleation process, while wire-like morphologies were obtained at low temperatures as normal concentration-dominated nucleation occurs. A Schottky SC-PSC based on the $MAPbBr_3$ sheets grown directly on ITO/FTO substrates and Au as the top electrode exhibited a power-conversion efficiency of 2.3%.

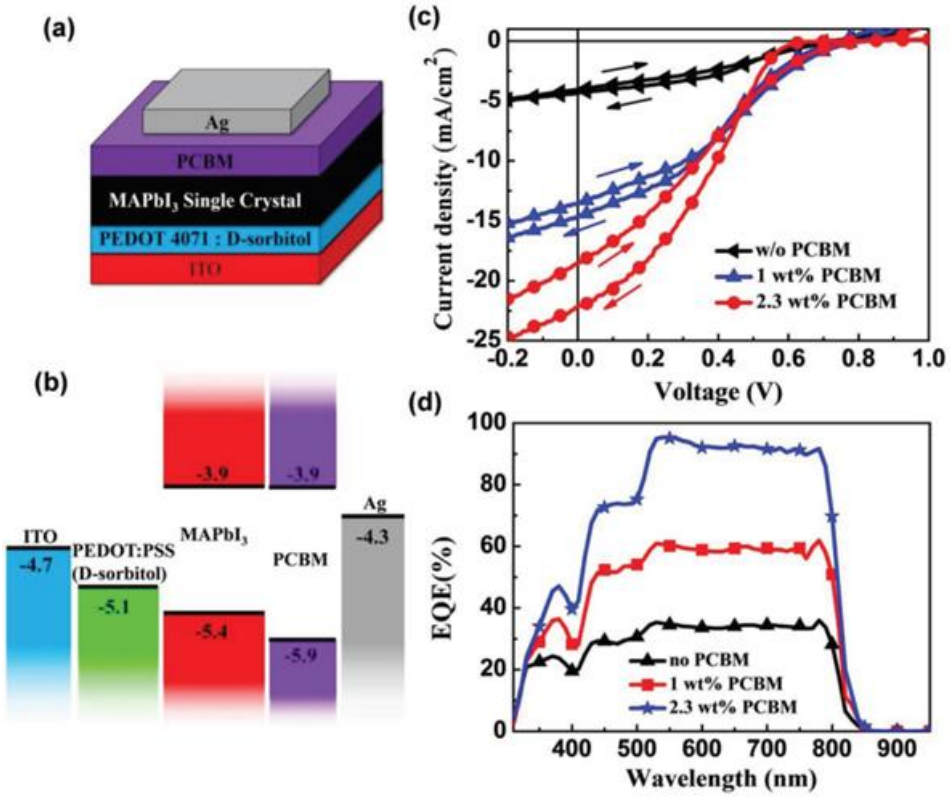

Figure 10. a) Device structure of the SC-PSC. b) Energy-level diagram of the materials used in this study. c) J–V curves of the various OPV devices, measured under the illumination of 1 sun.

d) Corresponding EQE spectra of the SC-PSC. Reproduced with permission.[116] Copyright 2018, Wiley-VCH.

Chen et al. fabricated SC-PSC with an efficiency of 4.4% and a maximum external quantum efficiency of 96%.[116] A seeded space-limited ITC technique was employed where a seed crystal of $MAPbI_3$ is placed between two substrates with confined space along with precursor solution. SC-PSC were fabricated by adhering the SC onto PEDOT:PSS coated ITO/PET substrates (**Figure 10**). A PCBM layer was coated on the top of the crystal by spin coating followed by an Ag electrode deposited through thermal evaporation. For devices with no PCBM layer, a low efficiency of 1.1% was achieved. However, devices with PCBM layers exhibited higher efficiency as well as better stability. In the first demonstration of such a technique, Li et al. employing space-limited temperature gradient technique to grow SC-$MAPbI_3$ on mesoporous (m)-TiO_2 to fabricate PSCs.[117] m-TiO_2 films were coated on compact (c)-TiO_2/FTO substrates and partially dipped inside precursor solution vertically. The capillary action drives the precursor solution upward into the space between the two substrates, akin to the wick of a candle. There is a temperature gradient established with the solution at the bottom hotter than at the top. The bottom-most solution maintains a saturated level due to high temperature, whereas the top-most solution is supersaturated as a result of relatively cooler temperature, leading to the formation of a single crystal of perovskite.[100] To fabricate SC-PSC, Spiro-OMeTAD and Ag were coated as the HTL layer and top electrode, respectively on the top of $MAPbI_3$ grown on m-TiO_2/c-TiO_2/FTO. 8.78% efficiency was recorded for the SC-PSC with a high J_{sc} of 22.1 mA/cm^2. It was found that the SC-$MAPbI_3$ does not cover the whole surface of m-TiO_2, which can result in direct contact between HTL and ETL layers, thereby reducing the device performance.

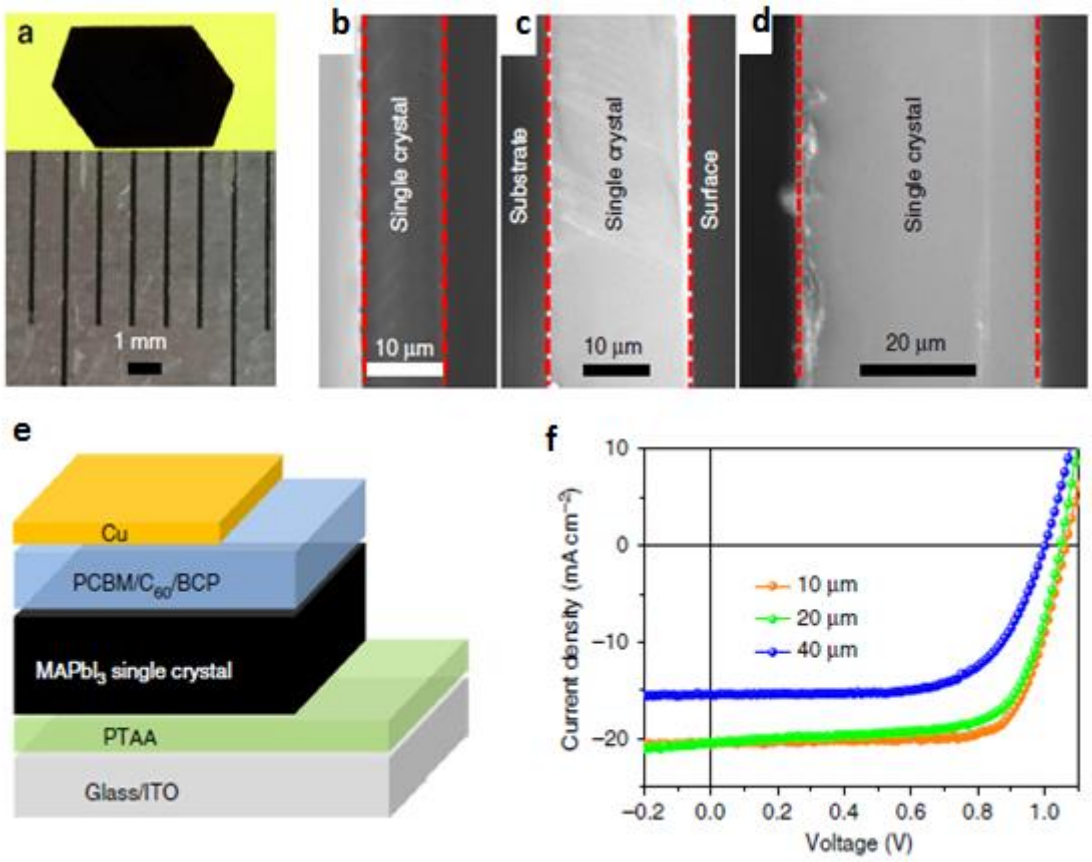

Figure 11. Characterization of perovskite thin single crystals. Photographs of a $MAPbI_3$ thin single crystal using the hydrophobic interface confined lateral growth method. Cross-sectional SEM images of the $MAPbI_3$ thin single crystals with different thickness: b) ≈10 μm, c) ≈20 μm, d) ≈40 μm. e) Device structure of the SC-PSC. f) Current density–voltage of the SC-PSC. Reproduced with permission.[24] Copyright 2017, Nature Publishing Group.

Similar to the hydrophobic substrate-driven nucleation of large-grained, polycrystalline films as mentioned earlier, Huang et al. took advantage of the hydrophobic nature of PTAA to grow thin SC-$MAPbI_3$ by space confined crystallization.[24] The hydrophobic PTAA layer accelerates the diffusion rate of precursor ions in the cavity between the two substrates. This enables continuous lateral growth of SC-$MAPbI_3$ up to several millimeters (**Figure 11**). In contrast, hydrophilic surfaces such as glass and ITO retard the diffusion rate due to surface tension. For the fabrication of SC-PSCs, PCBM/C60/BCP and Cu was deposited on the top of the $MAPbI_3$ crystals grown on PTAA/ITO as ETL and top contact, respectively. A high efficiency of 16.1%

was achieved for 10 µm thick crystals. To further improve the efficiency, the top surface of the crystals was coated with MAI prior to depositing the ETL layer. MAI passivates the surface traps leading to enhanced efficiency of 17.8% for the best device.

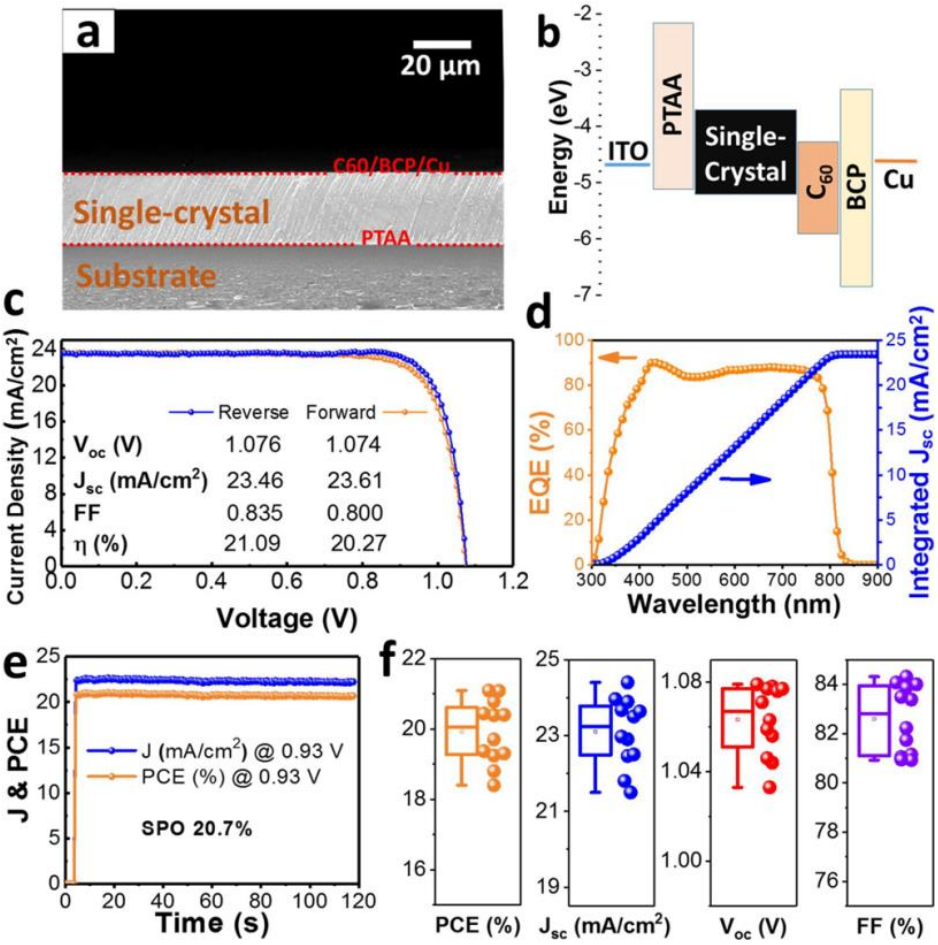

Figure 12. Characterization of SC-PSCs. a) Cross-sectional SEM image of a $MAPbI_3$ SC-PSCs. Note that the few nanometer-thick transporting layers at the crystal's two interfaces are not visible at such magnification. b) Energy-level diagram for SC-PSCs. c) J−V curves of the champion cell in forward- (orange) and reverse-scan (blue) modes and the corresponding photovoltaic parameters under 1 sun illumination. d) EQE spectra with the integrated JSC of the champion cell. e) Steady-state photocurrent and PCE output at maximum power point with 0.93 V bias for the champion cell. f) Statistical summary based on 12 devices, of the photovoltaic parameters of SC-PSCs. Reproduced with permission.[17] Copyright 2019, American Chemical Society.

In a recent breakthrough, Bakr et al. reported SC-PSCs with a record high efficiency of 21% along with an exceptionally high fill factor of 84%.[17] 20 µm $MAPbI_3$ crystals were directly

grown on PTAA HTL coated substrates by space-limited ITC technique. C60/BCP was coated on the top of the crystal as ETL, and then Cu was deposited as the top electrode (**Figure 12**). These SC-PSCs exhibited negligible hysteresis in the J-V curve. To date, this is the highest efficiency reported for SC-PSCs, which is on par with the polycrystalline PSCs. It was observed that the performance of SC-PSCs decreased drastically when exposed to ambient condition (22 °C, 50-55% RH), which was attributed to crystal surface hydration leading to inferior contact with charge transport layers.

Most of the SC-PSCs are based on pure I or Br-based single crystals. But recently, mixed-halide perovskite single crystals are slowing gaining attention. Zhou et al. explored mixed perovskite $(FAPbI_3)_{0.85}(MAPbBr_3)_{0.15}$ SC-PSCs and achieved an efficiency of 12.18%.[118] NiO_x and TiO_2 were employed as HTL and ETL, respectively in p-i-n device architecture. The crystals were grown by PDMS-assisted solvent evaporation where a PDMS layer is placed on the top of ITO/NiO_x and precursor solution is injected between the gap between PDMS and substrate. Upon heating to 80 °C for 2 hours, crystals of mixed perovskite with lateral dimensions of 500 μm to 2 mm appear on the substrate.

3.2. Lateral-Structure SC-PSCs

In addition to vertical-structure SC-PSCs, there have been a few reports on lateral SC-PSCs. The inherent advantage of lateral devices is their simple architecture and facile fabrication. In general, two planar electrodes are deposited on the top surface of the crystal. Three variations of the lateral-structure SC-PSCs are shown in **Figure 8b**. The simplest architecture consists of two planar electrodes of similar metal. In the second case, a charge transport layer is coated below one of the metal electrodes. In the third architecture, two dissimilar planar metal electrodes are deposited on the crystal surface in addition to the charge transport layer.

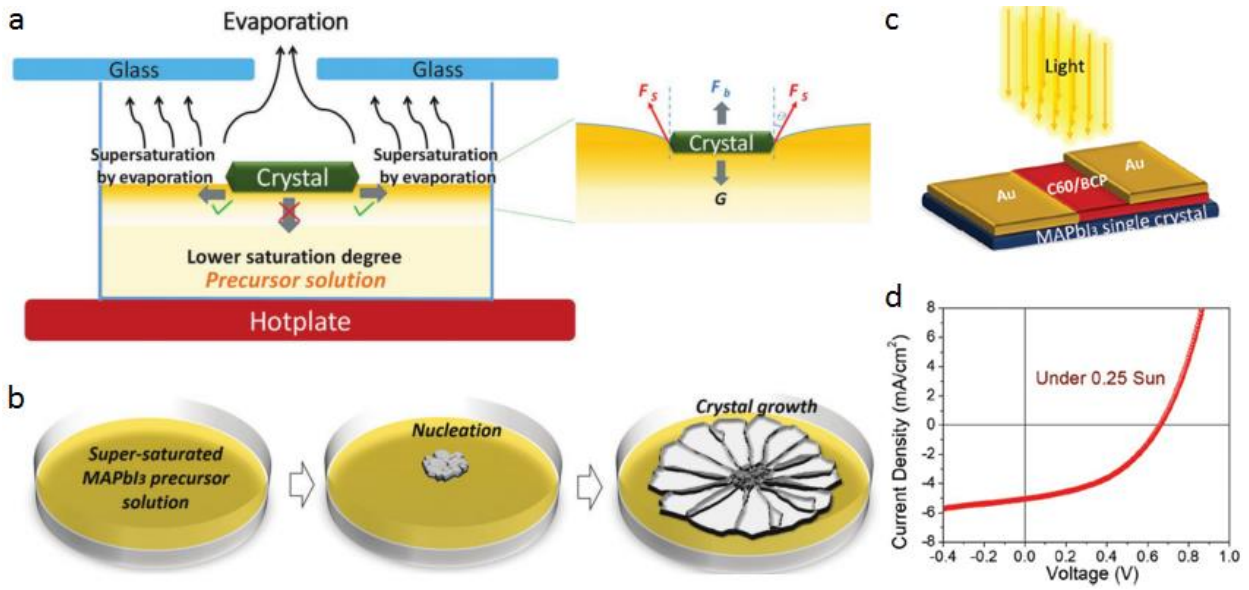

Figure 13. a,b) Scheme of crystal growth mechanism. c) Scheme of $MAPbI_3$ crystal-wafer lateral-structure solar cell device. d) The J–V curve of the best co-planar lateral $MAPbI_3$ single-crystal solar cell device with PCE of 5.9%. Reproduced with permission.[119] Copyright 2019, Wiley-VCH.

In one early work, Huang et al. developed lateral SC-PSC by depositing symmetrical Au co-planar electrodes on $MAPbI_3$ crystal.[101] It was observed that there was a negligible photovoltaic effect for the pristine crystal. However, electrical poling was employed to induce p-i-n regions in the crystal in order to generate the photovoltaic effect. Due to the absence of grain boundaries in single crystals, it is not straight forward to achieve p-i-n regions resulting from ion migration and self-doping effect. Interestingly, it was observed that $MAPbI_3$ crystals exhibit piezoelectric poling, which results in the formation of grain boundaries caused by crystal facture. During poling of the crystal, dense stripes were observed under application of bias which disappeared after poling bias was turned off. It was proposed that such stripes were caused by slipping of weakly bonded planes resulting in interfaces/ grain boundaries and dislocation lines facilitating ion migration. An efficiency of 1.8% and 5.3% was recorded for the lateral SC-PSC at 300 K and

170 K, respectively. Higher efficiencies at low-temperatures were recorded due to increased photocurrent resulting from reduced charge recombination and enhanced mobility.

In a subsequent work, Huang et al. developed a low-temperature crystal growth technique to grow centimeter size $MAPbI_3$ crystal wafers with μm thickness within 30 minutes.[119] In this method, using controlled evaporation of the precursor solution, the rate of nucleation as well as growth can be controlled (**Figure 13**). In brief, the nucleation starts at the center area on the top surface of the precursor solution and several nuclei grow outward laterally, eventually the inner side merging at the center resulting in multicrystals. The large surface area of these SCs allowed the fabrication of a lateral structure PSC, with C60/BCP as ETL and Au as contact electrode. An efficiency of 5.9% was recorded under 0.25 sun illumination, among the highest values reported for lateral-structure PSCs. Furthermore, this efficiency was achieved without any poling treatment of the perovskite layer.

For SC-PSCs to compete with their polycrystalline counterparts, it is imperative to develop scalable techniques for growing SC perovskites. In a crucial work, Sung et al. developed a roll-printing technique to grow large-area lateral SC patterns of $MAPbI_3$.[120] In this technique, perovskite ink is transferred to the heated substrate using a patterned roller resulting in geometrically confined, unidirectional crystal growth (**Figure 14**). High carrier mobility of 45.6 $cm^2V^{-1}s^{-1}$ was measured for these patterned $MAPbI_3$ structures. Furthermore, these patterns were employed in a lateral-structure solar cell by depositing a charge transport layer (PCBM) and Au and Ag electrodes. To achieve p-i-n structure in the perovskite layer, polling was performed prior to efficiency measurements. The SC-PSC exhibited an efficiency of 4.8% in contrast to 0.19% for the polycrystalline film based lateral PSC under one sun illumination. While such lateral devices may not compete with vertical devices in terms of efficiency, they might be useful for

powering small electronic devices and for integration with other devices due to their facile fabrication and simple architecture.

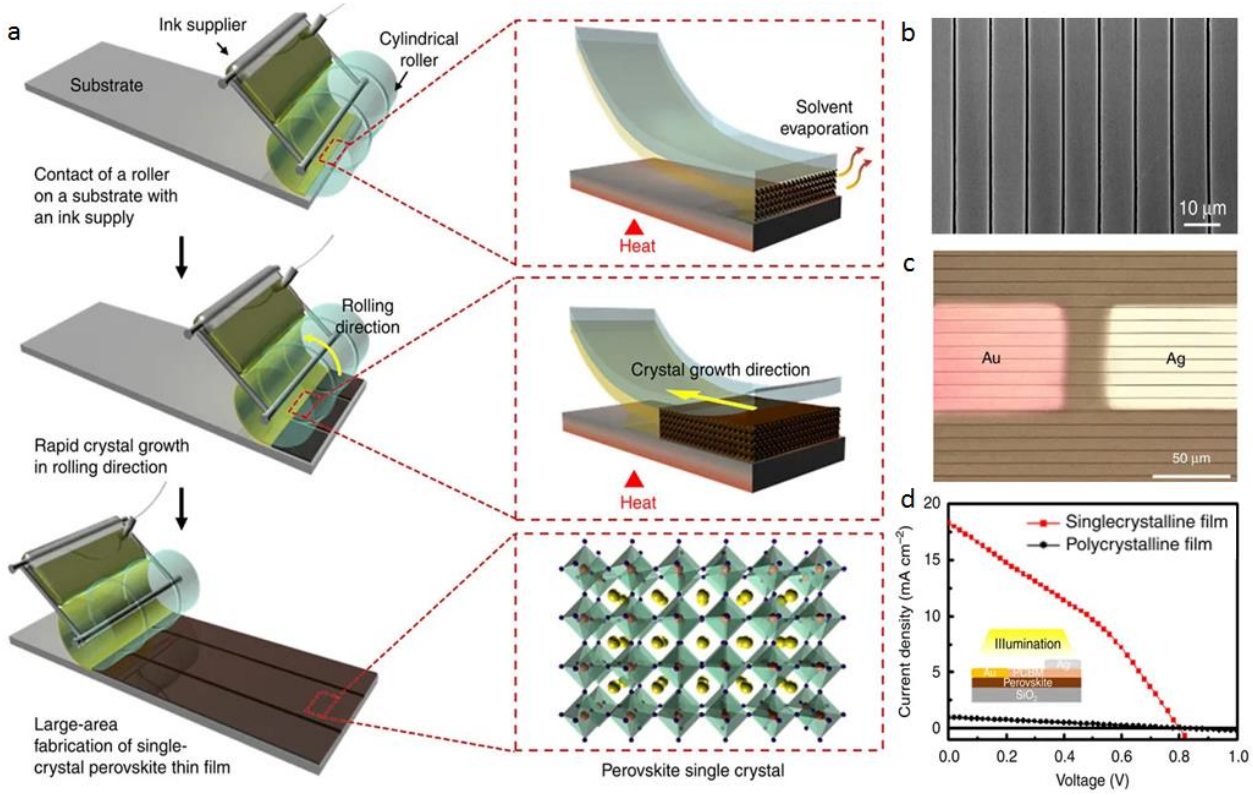

Figure 14. Fabrication of single-crystal perovskite patterned thin films. a) Schematic of the manufacturing procedure for single-crystal perovskite thin films using geometrically confined lateral crystal growth with a rolling mould. b) SEM image of single-crystal perovskite patterned thin film consisting of 10-μm-wide strips with 400-nm-wide spacing. c) An optical microscopic image of a single-crystal perovskite lateral perovskite solar cell with metal electrodes. The light brown and dark brown lines indicate perovskite single crystals and spaces, respectively. d) J–V curves of SC (red) and polycrystalline (black) perovskite thin film lateral perovskite solar cells. The inset shows a schematic device structure of a lateral perovskite solar cell and the direction of illumination. Reproduced with permission.[120] Copyright 2017, Nature Publishing Group.

Various architectures of SC-PSCs and their corresponding performance are summarized in **Table 2**. While both *n-i-p* and *p-i-n* device architectures have been explored for SC-PSCs, higher efficiencies (> 10%) are mainly realized for *p-i-n* SC-PSCs. Similar to polycrystalline PSCs, a number of charge transport layers (ETL/HTL) such as TiO_2, PCBM, C60, Spiro-OMeTAD, NiO_x have been employed for SC-PSCs. Interestingly, the best efficiencies in SC-PSCs were achieved

when both the ETL/HTL layers were organic. In particular, PTAA as HTL and PCBM, C_{60} as ETL serve as efficient charge transport layers for SC-PSCs. In terms of single crystal growth techniques for SC-PSCs, the best efficiencies were obtained by space confined growth approaches such as hydrophobic interface confined crystallization and space confined ITC. While large perovskite single crystals have been demonstrated, the device areas of SC-PSCs are relatively small compared to polycrystalline PSCs, which demands more attention for their further development.

Table 2: Some representative works on state-of-the art SC-PSCs with structure and performance details.

Perovskite	Crystal growth method	Crystal thickness	Device architecture	Device Area (cm^2)	Device structure	η (%)	Year	Ref
$MAPbI_3$	Droplet-pinned crystallization	~3 µm	*p-i-n*	-		1.73	2015	[112]
$MAPbI_3$	Seeded solution growth	-	*p-i-n*	-		~ 4	2017	[113]
$MAPbI_3$	Space confined gradient temperature	-	*n-i-p*	0.01		8.78	2017	[117]
$MAPbI_3$	Hydrophobic interface confined crystallization	10 µm	*p-i-n*	-		17.8	2017	[24]
$MAPbI_3$	Seeded space-limited ITC	50 µm	*p-i-n*	-		4.4	2018	[116]
$MAPbI_3$	Space-limited ITC	~20 µm	*p-i-n*	0.01		21.09	2019	[17]
$MAPbI_3$	Temperature lowering	Bulk	-	0.0005		1.88	2016	[101]
$MAPbI_3$	Geometrically confined roll-	200 nm	-	$23x10^{-6}$		4.83	2017	[120]

	printing						
$MAPbI_3$	Controlled precursor solution evaporation	Tens of micron	-	$364x10^{-6}$		5.9	2019 [119]
$MAPbBr_3$	cavitation-triggered asymmetrical crystallization	1 µm	*n-i-p*	0.2		6.53	2016 [98]
$MAPbBr_3$	Space-limited ITC	16 µm	*n-i-p*	-		7.11	2017 [114]
$MAPbBr_3$	Space-limited crystallization	15 µm	*n-i-p*	-		2.3	2018 [115]
$(FAPbI_3)_{0.85}(MAPbBr_3)_{0.15}$	Solvent evaporation	24.5 µm	*p-i-n*	0.00316		12.18	2018 [118]

4. Conclusions and Outlook

In this review, we have discussed the emerging large grain PSCs and SC-PSCs in terms of different hybrid perovskite compositions and device architectures. Due to the strong relation between perovskite film quality and its photophysical properties, significant efforts are directed towards its improvement. The combination of suitable additives and techniques are able to produce high-quality films on relatively large substrates with superior structural, morphological, and electrical properties. Facile growth enabled SC-PSCs are also now competing with polycrystalline PSCs in terms of efficiency. Despite the efficiency of polycrystalline and SC-PSCs reaching above 20%, there still remain several challenges to overcome. We anticipate future advances in the direction of more stable compositions, advanced device architectures, and scalable growth techniques.

With perovskite solar cell efficiency approaching the point of diminishing returns, the stability of such materials must now receive increased attention in order to make this class of

solar cell technology viable. While large grain perovskite films exhibit enhanced stability compared to small grain films owing to low grain boundary area, the required stability level for long term usage is still yet to be realized. In case of SC-PSCs, enhanced stability has been observed compared to polycrystalline PSCs due to the absence of grain boundaries.[24] But more robust, long-term stability tests must be designed to prove the usefulness of SC-PSCs over polycrystalline counterparts. SC-PSCs can improve the understanding on the issue of hysteresis[121-122] and ion migration[123-124] and elucidate the role of grain boundaries in observation of such phenomena. Further stability improvement can be achieved by additive engineering of perovskites: Incorporation of additives with ion blocking character into perovskites will be a significant step for tackling the issue of ion migration at grain boundaries. Also, additives with the ability to enhance the moisture stability of perovskites should be explored for more robust PSCs. Low dimensional perovskites such as 2D halide perovskites have attracted significant attention for being relatively more stable than 3D counterparts.[125-127] Similar to 3D halide perovskites, strategies such as additive engineering have been also applied to polycrystalline 2D perovskite PSCs to further improve the stability and efficiency.[128-130] While large-size single crystals and membranes of 2D perovskites have been already demonstrated, they remain to be explored for SC-PSCs.[131] Recent reports on phenethylammonium (PEA) cation-based 2D perovskite single crystals demonstrate that the optoelectronic properties are on par with 3D perovskites with MA, FA, or Cs cation.[132-133] Harnessing the combination of enhanced stability of single crystals with intrinsic stability of 2D perovskites for SC-PSCs will be an interesting direction for future exploration.

In terms of device architecture, a variety of architectures have been explored for polycrystalline PSCs with different charge transport layers and interfacial engineering to achieve

high performance. For SC-PSCs, traditional vertical device architecture similar to films based PSCs have been successful in crossing the 20% efficiency mark. Growing perovskite single crystals directly on the top silicon solar cells can further boost the efficiency of such tandem devices. Another possibility is to coat SC perovskite layer on silicon solar cells by scalable techniques such as geometrically confined unidirectional crystal growth.[120] Lateral SC-PSCs are still below 6% efficiency mark possibly, due to surface and interfacial charge recombination.[119] Engineered interfaces with high performance charge transport layer can be explored for further improvement of lateral SC-PSCs.

Finally, developing scalable techniques of depositing high-quality polycrystalline perovskite films as well as large thin single crystals is of critical importance. Blade coating is one viable technique with low material wastage and compatibility with roll to roll printing. Recent work suggests that blade coating with the aid of surfactants or additives is among the most efficient technique of fabricating scalable PSCs.[80] In spite of the great advantages offered by perovskite single crystals, large-area devices remain unexplored. SC perovskite films on substrates are more suitable for SC-PSCs. In one work, 120 cm^2 $MAPbBr_3$ SC-film on FTO was grown by space limited ITC technique for photodetection.[134] Also, large wafers of SC-$MAPbI_3$ have been reported, which potentially can be explored for lateral SC-PSC modules.[102]

With the amount of research effort invested into the processing of high quality, large-grain polycrystalline perovskite films, it is no wonder their performance in solar cells has risen to the heights currently achieved with relatively simple fabrication techniques. This begs the question: Are these polycrystalline films already “good enough” in comparison to single crystals? We have highlighted the intrinsic benefits of single crystals over polycrystalline films – reductions in defect density and ion migration. It is conceivable that perovskite single crystals could be

fabricated at a similar size to conventional 130-150 mm silicon wafers and processed into cells, which could then be "tiled" into modules. To achieve the same from solution-processed polycrystalline films would require intensive process control in order to eliminate pinholes and ensure uniformity across a very large area film.

Currently, spin-coating is heavily relied upon to achieve the high-quality polycrystalline films associated with ground-breaking PCEs. However, the applicability of spin-coating is reduced at the areas required for commercialization, given an increase in defect formation and materials wastage. Other coating techniques have, so far, not been able to match the performance of spin-coated films.[135] If perovskite single-crystal growth techniques are further improved, this approach of upscaling may prove preferable to polycrystalline methods, given the benefits of SC-PSCs. However, we stress that this can only become a reality with future improvements in crystal production, device stability, and efficiency. Indeed, large area SC-PSCs and modules will be next important step toward the applicability of perovskite single crystals and may well be the future of perovskite photovoltaics: The current record efficiency competitors to perovskite-based technologies include GaAs and Silicon. These technologies share the properties of being processed using a single crystal of their respective material, whether it be from a sliced boule or grown using epitaxial CVD. The preference for single crystals over polycrystalline structures is the same for these technologies as it is for perovskites - The reduction of defects. Where SC-PSCs can shine, therefore, lies in their ease of processing and reduced embodied energy given their solution-processed nature.

Acknowledgment

This publication is based upon work supported by the King Abdullah University of Science and Technology (KAUST) Office of Sponsored Research (OSR) under Award No. OSR-CRG2018-3737.

Received: ((will be filled in by the editorial staff))
Revised: ((will be filled in by the editorial staff))
Published online: ((will be filled in by the editorial staff))

References

[1] N. R. E. L. Best Research-Cell Efficiencies, www.nrel.gov/ncpv/images/efficiency chart.jpg. (Accessed: August, 2019)
[2] M. Gratzel, *Nat. Mater.* **2014,** *13*, 838.
[3] M. A. Green, A. Ho-Baillie, H. J. Snaith, *Nat. Photonics* **2014,** *8*, 506.
[4] D. Shi, V. Adinolfi, R. Comin, M. Yuan, E. Alarousu, A. Buin, Y. Chen, S. Hoogland, A. Rothenberger, K. Katsiev, Y. Losovyj, X. Zhang, P. A. Dowben, O. F. Mohammed, E. H. Sargent, O. M. Bakr, *Science* **2015,** *347*, 519.
[5] S. D. Stranks, G. E. Eperon, G. Grancini, C. Menelaou, M. J. Alcocer, T. Leijtens, L. M. Herz, A. Petrozza, H. J. Snaith, *Science* **2013,** *342*, 341.
[6] G. Xing, N. Mathews, S. Sun, S. S. Lim, Y. M. Lam, M. Gratzel, S. Mhaisalkar, T. C. Sum, *Science* **2013,** *342*, 344.
[7] Q. Dong, Y. Fang, Y. Shao, P. Mulligan, J. Qiu, L. Cao, J. Huang, *Science* **2015,** *347*, 967.
[8] X. Zheng, J. Troughton, N. Gasparini, Y. Lin, M. Wei, Y. Hou, J. Liu, K. Song, Z. Chen, C. Yang, B. Turedi, A. Y. Alsalloum, J. Pan, J. Chen, A. A. Zhumekenov, T. D. Anthopoulos, Y. Han, D. Baran, O. F. Mohammed, E. H. Sargent, O. M. Bakr, *Joule* **2019**, 3, 1963.
[9] J. Troughton, N. Gasparini, D. Baran, *J. Mater. Chem. A* **2018,** *6*, 21913.
[10] L. Zheng, D. Zhang, Y. Ma, Z. Lu, Z. Chen, S. Wang, L. Xiao, Q. Gong, *Dalton Trans.* **2015,** *44*, 10582.
[11] N. J. Jeon, J. H. Noh, Y. C. Kim, W. S. Yang, S. Ryu, S. II Seok, *Nat. Mater.* **2014,** *13*, 897.
[12] M. Liu, M. B. Johnston, H. J. Snaith, *Nature* **2013,** *501*, 395.
[13] Q. Chen, H. Zhou, Z. Hong, S. Luo, H. S. Duan, H. H. Wang, Y. Liu, G. Li, Y. Yang, *J. Am. Chem. Soc.* **2014,** *136*, 622.
[14] M. A. Haque, A. D. Sheikh, X. Guan, T. Wu, *Adv. Energy Mater.* **2017**, 7, 1602803.
[15] L. Huang, Z. Ge, *Adv. Energy Mater.* **2019,** *9*, 1900248.
[16] Y. Wang, M. Li, H. Li, Y. Lan, X. Zhou, C. Li, X. Hu, Y. Song, *Adv. Energy Mater.* **2019**, 1900838.
[17] Z. Chen, B. Turedi, A. Y. Alsalloum, C. Yang, X. Zheng, I. Gereige, A. AlSaggaf, O. F. Mohammed, O. M. Bakr, *ACS Energy Lett.* **2019,** *4*, 1258.
[18] B. Yang, O. Dyck, J. Poplawsky, J. Keum, A. Puretzky, S. Das, I. Ivanov, C. Rouleau, G. Duscher, D. Geohegan, K. Xiao, *J. Am. Chem. Soc.* **2015,** *137*, 9210.
[19] S. Y. Leblebici, L. Leppert, Y. Li, S. E. Reyes-Lillo, S. Wickenburg, E. Wong, J. Lee, M. Melli, D. Ziegler, D. K. Angell, D. F. Ogletree, Paul D. Ashby, F. M. Toma, J. B. Neaton, I. D. Sharp, A. Weber-Bargioni, *Nat. Energy* **2016,** *1*, 16093.
[20] G. Maculan, A. D. Sheikh, A. L. Abdelhady, M. I. Saidaminov, M. A. Haque, B. Murali, E. Alarousu, O. F. Mohammed, T. Wu, O. M. Bakr, *J. Phys. Chem. Lett.* **2015,** *6*, 3781.
[21] P. A. Shaikh, D. Shi, J. R. D. Retamal, A. D. Sheikh, M. A. Haque, C.-F. Kang, J.-H. He, O. M. Bakr, T. Wu, *J. Mater. Chem. C* **2016,** *4*, 8304.
[22] Y. Fang, Q. Dong, Y. Shao, Y. Yuan, J. Huang, *Nat. Photonics* **2015,** *9*, 679.

[23] H. Wei, Y. Fang, P. Mulligan, W. Chuirazzi, H.-H. Fang, C. Wang, B. R. Ecker, Y. Gao, M. A. Loi, L. Cao, J. Huang, *Nat. Photonics* **2016,** *10*, 333.
[24] Z. Chen, Q. Dong, Y. Liu, C. Bao, Y. Fang, Y. Lin, S. Tang, Q. Wang, X. Xiao, Y. Bai, Y. Deng, J. Huang, *Nat. Commun.* **2017,** *8*, 1890.
[25] S. Yakunin, M. Sytnyk, D. Kriegner, S. Shrestha, M. Richter, G. J. Matt, H. Azimi, C. J. Brabec, J. Stangl, M. V. Kovalenko, W. Heiss, *Nat. Photonics* **2015,** *9*, 444.
[26] H. Zhu, Y. Fu, F. Meng, X. Wu, Z. Gong, Q. Ding, M. V. Gustafsson, M. T. Trinh, S. Jin, X. Y. Zhu, *Nat. Mater.* **2015,** *14*, 636.
[27] S. D. Stranks, H. J. Snaith, *Nat. Nanotechnol.* **2015,** *10*, 391.
[28] I. Dursun, Y. Zheng, T. Guo, M. De Bastiani, B. Turedi, L. Sinatra, M. A. Haque, B. Sun, A. A. Zhumekenov, M. I. Saidaminov, F. P. García de Arquer, E. H. Sargent, T. Wu, Y. N. Gartstein, O. M. Bakr, O. F. Mohammed, A. V. Malko, *ACS Energy Lett.* **2018,** *3*, 1492.
[29] M. Saliba, T. Matsui, J. Y. Seo, K. Domanski, J. P. Correa-Baena, M. K. Nazeeruddin, S. M. Zakeeruddin, W. Tress, A. Abate, A. Hagfeldt, M. Gratzel, *Energy Environ. Sci.* **2016,** *9*, 1989.
[30] M. H. Shang, J. Zhang, P. Zhang, Z. Yang, J. Zheng, M. A. Haque, W. Yang, S. H. Wei, T. Wu, *J. Phys. Chem. Lett.* **2019**, 10, 59.
[31] C. Wang, Z. Song, C. Li, D. Zhao, Y. Yan, *Adv. Funct. Mater.* **2019**, 1808801.
[32] F. Hao, C. C. Stoumpos, D. H. Cao, R. P. H. Chang, M. G. Kanatzidis, *Nat. Photonics* **2014,** *8*, 489.
[33] G. Grancini, M. K. Nazeeruddin, *Nat. Rev. Mater.* **2018,** *4*, 4.
[34] N.-G. Park, M. Grätzel, T. Miyasaka, K. Zhu, K. Emery, *Nat. Energy* **2016,** *1*, 16152.
[35] H. Zhou, Q. Chen, G. Li, S. Luo, T.-b. Song, H.-S. Duan, Z. Hong, J. You, Y. Liu, Y. Yang, *Science* **2014,** *345*, 542.
[36] J. Burschka, N. Pellet, S. J. Moon, R. Humphry-Baker, P. Gao, M. K. Nazeeruddin, M. Gratzel, *Nature* **2013,** *499*, 316.
[37] A. D. Sheikh, R. Munir, M. A. Haque, A. Bera, W. Hu, P. Shaikh, A. Amassian, T. Wu, *ACS Appl. Mater. Interfaces* **2017,** *9*, 35018.
[38] W. Nie, H. Tsai, R. Asadpour, J.-C. Blancon, A. J. Neukirch, G. Gupta, J. J. Crochet, M. Chhowalla, S. Tretiak, M. A. Alam, H.-L. Wang, A. D. Mohite, *Science* **2015,** *347*, 522.
[39] N. Ahn, D. Y. Son, I. H. Jang, S. M. Kang, M. Choi, N. G. Park, *J. Am. Chem. Soc.* **2015,** *137*, 8696.
[40] P. W. Liang, C. Y. Liao, C. C. Chueh, F. Zuo, S. T. Williams, X. K. Xin, J. Lin, A. K. Jen, *Adv. Mater.* **2014,** *26*, 3748.
[41] M. A. Haque, M. I. Nugraha, S. H. K. Paleti, D. Baran, *J. Phys. Chem. C* **2019,** *123*, 14928.
[42] B. Dänekamp, C. Müller, M. Sendner, P. P. Boix, M. Sessolo, R. Lovrincic, H. J. Bolink, *J. Phys. Chem. Lett.* **2018,** *9*, 2770.
[43] M. M. Lee, J. Teuscher, T. Miyasaka, T. N. Murakami, H. J. Snaith, *Science* **2012,** *338*, 643.
[44] Masanao Era, Toshihiko Hattori, Takahiro Taira, T. Tsutsui, *Chem. Mater.* **1997,** *9*, 8.
[45] G. Grancini, A. R. Srimath Kandada, J. M. Frost, A. J. Barker, M. De Bastiani, M. Gandini, S. Marras, G. Lanzani, A. Walsh, A. Petrozza, *Nat. Photonics* **2015,** *9*, 695.
[46] J. W. Lee, H. S. Kim, N. G. Park, *Acc. Chem. Res.* **2016,** *49*, 311.
[47] Q. Wang, B. Chen, Y. Liu, Y. Deng, Y. Bai, Q. Dong, J. Huang, *Energy Environ. Sci.* **2017,** *10*, 516.
[48] M. A. Haque, A. Syed, F. H. Akhtar, R. Shevate, S. Singh, K. V. Peinemann, D. Baran, T. Wu, *ACS Appl. Mater. Interfaces* **2019**, 11, 29821.

[49] Y. Shao, Y. Fang, T. Li, Q. Wang, Q. Dong, Y. Deng, Y. Yuan, H. Wei, M. Wang, A. Gruverman, J. Shield, J. Huang, *Energy Environ. Sci.* **2016,** *9*, 1752.
[50] J. H. Im, I. H. Jang, N. Pellet, M. Gratzel, N. G. Park, *Nat. Nanotechnol.* **2014,** *9*, 927.
[51] F. Huang, Y. Dkhissi, W. Huang, M. Xiao, I. Benesperi, S. Rubanov, Y. Zhu, X. Lin, L. Jiang, Y. Zhou, A. Gray-Weale, J. Etheridge, C. R. McNeill, R. A. Caruso, U. Bach, L. Spiccia, Y.-B. Cheng, *Nano Energy* **2014,** *10*, 10.
[52] S. Bae, J. W. Jo, P. Lee, M. J. Ko, *ACS Appl. Mater. Interfaces* **2019,** *11*, 17452.
[53] Y. Liu, I. Shin, I. W. Hwang, S. Kim, J. Lee, M. S. Yang, Y. K. Jung, J. W. Jang, J. H. Jeong, S. H. Park, K. H. Kim, *ACS Appl. Mater. Interfaces* **2017,** *9*, 12382.
[54] H. J. Yen, P. W. Liang, C. C. Chueh, Z. Yang, A. K. Jen, H. L. Wang, *ACS Appl. Mater. Interfaces* **2016,** *8*, 14513.
[55] W. S. Yang, J. H. Noh, N. J. Jeon, Y. C. Kim, S. Ryu, J. Seo, S. I. Seok, *Science* **2015,** *348*, 1234.
[56] X. Li, D. Bi, C. Yi, J.-D. Décoppet, J. Luo, S. M. Zakeeruddin, A. Hagfeldt, M. Grätzel, *Science* **2016**, 353, 58.
[57] S. Tang, Y. Deng, X. Zheng, Y. Bai, Y. Fang, Q. Dong, H. Wei, J. Huang, *Adv. Energy Mater.* **2017,** *7*, 1700302.
[58] X. Ren, Z. Yang, D. Yang, X. Zhang, D. Cui, Y. Liu, Q. Wei, H. Fan, S. F. Liu, *Nanoscale* **2016,** *8*, 3816.
[59] H. Tsai, W. Nie, P. Cheruku, N. H. Mack, P. Xu, G. Gupta, A. D. Mohite, H.-L. Wang, *Chem. Mater.* **2015,** *27*, 5570.
[60] D. Bi, C. Yi, J. Luo, J.-D. Décoppet, F. Zhang, Shaik M. Zakeeruddin, X. Li, A. Hagfeldt, M. Grätzel, *Nat. Energy* **2016,** *1*, 16142.
[61] G. W. P. Adhyaksa, S. Brittman, H. Abolins, A. Lof, X. Li, J. D. Keelor, Y. Luo, T. Duevski, R. M. A. Heeren, S. R. Ellis, D. P. Fenning, E. C. Garnett, *Adv. Mater.* **2018,** *30*, 1804792.
[62] H.-C. Liao, P. Guo, C.-P. Hsu, M. Lin, B. Wang, L. Zeng, W. Huang, C. M. M. Soe, W.-F. Su, M. J. Bedzyk, M. R. Wasielewski, A. Facchetti, R. P. H. Chang, M. G. Kanatzidis, T. J. Marks, *Adv. Energy Mater.* **2017,** *7*, 1601660.
[63] M. Kim, G.-H. Kim, T. K. Lee, I. W. Choi, H. W. Choi, Y. Jo, Y. J. Yoon, J. W. Kim, J. Lee, D. Huh, H. Lee, S. K. Kwak, J. Y. Kim, D. S. Kim, *Joule* **2019**, 3, 2179.
[64] C. Qin, T. Matsushima, T. Fujihara, C. Adachi, *Adv. Mater.* **2017,** *29*, 1603808.
[65] H. Li, G. Wu, W. Li, Y. Zhang, Z. Liu, D. Wang, S. F. Liu, *Adv. Sci.* **2019**, 1901241.
[66] D. Bi, X. Li, J. V. Milic, D. J. Kubicki, N. Pellet, J. Luo, T. LaGrange, P. Mettraux, L. Emsley, S. M. Zakeeruddin, M. Gratzel, *Nat. Commun.* **2018,** *9*, 4482.
[67] Y. Wu, F. Xie, H. Chen, X. Yang, H. Su, M. Cai, Z. Zhou, T. Noda, L. Han, *Adv. Mater.* **2017,** *29*, 1701073.
[68] W. Ke, C. Xiao, C. Wang, B. Saparov, H. S. Duan, D. Zhao, Z. Xiao, P. Schulz, S. P. Harvey, W. Liao, W. Meng, Y. Yu, A. J. Cimaroli, C. S. Jiang, K. Zhu, M. Al-Jassim, G. Fang, D. B. Mitzi, Y. Yan, *Adv. Mater.* **2016,** *28*, 5214.
[69] Y. Yang, H. Peng, C. Liu, Z. Arain, Y. Ding, S. Ma, X. Liu, T. Hayat, A. Alsaedi, S. Dai, *J. Mater. Chem. A* **2019,** *7*, 6450.
[70] L. Li, Y. Chen, Z. Liu, Q. Chen, X. Wang, H. Zhou, *Adv. Mater.* **2016,** *28*, 9862.
[71] L. Zuo, Z. Gu, T. Ye, W. Fu, G. Wu, H. Li, H. Chen, *J. Am. Chem. Soc.* **2015,** *137*, 2674.

[72] Konrad Wojciechowski, Samuel D. Stranks, Antonio Abate, Golnaz Sadoughi, Aditya Sadhanala, Nikos Kopidakis, Garry Rumbles, Chang-Zhi Li, Richard H. Friend, Alex K.-Y. Jen, H. J. Snaith, *ACS Nano* **2014,** *8*, 12701.
[73] Z. Zhou, S. Pang, Z. Liu, H. Xu, G. Cui, *J. Mater. Chem. A* **2015,** *3*, 19205.
[74] H. P. Dong, Y. Li, S. F. Wang, W. Z. Li, N. Li, X. D. Guo, L. D. Wang, *J. Mater. Chem. A* **2015,** *3*, 9999.
[75] W. Deng, X. Liang, P. S. Kubiak, P. J. Cameron, *Adv. Energy Mater.* **2017**, 1701544.
[76] C. Bi, Q. Wang, Y. Shao, Y. Yuan, Z. Xiao, J. Huang, *Nat. Commun.* **2015,** *6*, 7747.
[77] Z. G. Xiao, C. Bi, Y. C. Shao, Q. F. Dong, Q. Wang, Y. B. Yuan, C. G. Wang, Y. L. Gao, J. S. Huang, *Energy Environ. Sci.* **2014,** *7*, 2619.
[78] M. Hu, C. Bi, Y. Yuan, Y. Bai, J. Huang, *Adv. Sci.* **2016,** *3*, 1500301.
[79] X. Liu, Y. Cheng, C. Liu, T. Zhang, N. Zhang, S. Zhang, J. Chen, Q. Xu, J. Ouyang, H. Gong, *Energy Environ. Sci.* **2019,** *12*, 1622.
[80] Y. Deng, X. Zheng, Y. Bai, Q. Wang, J. Zhao, J. Huang, *Nat. Energy* **2018,** *3*, 560.
[81] X. Zheng, B. Chen, J. Dai, Y. Fang, Y. Bai, Y. Lin, H. Wei, Xiao C. Zeng, J. Huang, *Nat. Energy* **2017,** *2*, 17102.
[82] Y. Deng, E. Peng, Y. Shao, Z. Xiao, Q. Dong, J. Huang, *Energy Environ. Sci.* **2015,** *8*, 1544.
[83] Y. Deng, Q. Wang, Y. Yuan, J. Huang, *Mater. Horizons* **2015,** *2*, 578.
[84] M. He, B. Li, X. Cui, B. Jiang, Y. He, Y. Chen, D. O'Neil, P. Szymanski, M. A. Ei-Sayed, J. Huang, Z. Lin, *Nat. Commun.* **2017,** *8*, 16045.
[85] H. Ishihara, W. Chen, Y.-C. Chen, S. Sarang, N. De Marco, O. Lin, S. Ghosh, V. Tung, *Adv. Mater. Interfaces* **2016,** *3*, 1500762.
[86] S. Wang, Z. Ma, B. Liu, W. Wu, Y. Zhu, R. Ma, C. Wang, *Sol. RRL* **2018,** *2*, 1800034.
[87] T. M. Brenner, D. A. Egger, L. Kronik, G. Hodes, D. Cahen, *Nat. Rev. Mater.* **2016,** *1*, 15007.
[88] H. L. Wells, *Z. Anorg. Chem* **1893,** *3*, 195.
[89] C. K. Moller, *Nature* **1958,** *182*, 1436.
[90] D. Weber, *Z. Naturforsch.* **1978,** *33b*, 1443.
[91] D. Weber, *Z. Naturforsch.* **1978,** *33b*, 862.
[92] C. R. Kagan, D. B. Mitzi, C. D. Dimitrakopoulos, *Science* **1991,** *286*, 945.
[93] Y. Lei, Y. Chen, Y. Gu, C. Wang, Z. Huang, H. Qian, J. Nie, G. Hollett, W. Choi, Y. Yu, N. Kim, C. Wang, T. Zhang, H. Hu, Y. Zhang, X. Li, Y. Li, W. Shi, Z. Liu, M. J. Sailor, L. Dong, Y. H. Lo, J. Luo, S. Xu, *Adv. Mater.* **2018,** *30*, 1705992.
[94] Y. Liu, Y. Zhang, Z. Yang, J. Feng, Z. Xu, Q. Li, M. Hu, H. Ye, X. Zhang, M. Liu, K. Zhao, S. Liu, *Mater. Today* **2019,** *22*, 67.
[95] A. A. Zhumekenov, M. I. Saidaminov, M. A. Haque, E. Alarousu, S. P. Sarmah, B. Murali, I. Dursun, X.-H. Miao, A. L. Abdelhady, T. Wu, O. F. Mohammed, O. M. Bakr, *ACS Energy Lett.* **2016,** *1*, 32.
[96] Y. Liu, Z. Yang, D. Cui, X. Ren, J. Sun, X. Liu, J. Zhang, Q. Wei, H. Fan, F. Yu, X. Zhang, C. Zhao, S. F. Liu, *Adv. Mater.* **2015,** *27*, 5176.
[97] M. I. Saidaminov, A. L. Abdelhady, B. Murali, E. Alarousu, V. M. Burlakov, W. Peng, I. Dursun, L. Wang, Y. He, G. Maculan, A. Goriely, T. Wu, O. F. Mohammed, O. M. Bakr, *Nat. Commun.* **2015,** *6*, 7586.

[98] W. Peng, L. Wang, B. Murali, K. T. Ho, A. Bera, N. Cho, C. F. Kang, V. M. Burlakov, J. Pan, L. Sinatra, C. Ma, W. Xu, D. Shi, E. Alarousu, A. Goriely, J. H. He, O. F. Mohammed, T. Wu, O. M. Bakr, *Adv. Mater.* **2016,** *28*, 3383.
[99] Z. Gu, Z. Huang, C. Li, M. Li, Y. Song, *Sci. Adv.* **2018,** *4*, 2390.
[100] Y. X. Chen, Q. Q. Ge, Y. Shi, J. Liu, D. J. Xue, J. Y. Ma, J. Ding, H. J. Yan, J. S. Hu, L. J. Wan, *J. Am. Chem. Soc.* **2016,** *138*, 16196.
[101] Q. Dong, J. Song, Y. Fang, Y. Shao, S. Ducharme, J. Huang, *Adv. Mater.* **2016,** *28*, 2816.
[102] Y. Liu, Y. Zhang, Z. Yang, D. Yang, X. Ren, L. Pang, S. F. Liu, *Adv. Mater.* **2016,** *28*, 9204.
[103] M. I. Saidaminov, A. L. Abdelhady, G. Maculan, O. M. Bakr, *Chem. Commun.* **2015,** *51*, 17658.
[104] A. A. Zhumekenov, V. M. Burlakov, M. I. Saidaminov, A. Alofi, M. A. Haque, B. Turedi, B. Davaasuren, I. Dursun, N. Cho, A. M. El-Zohry, M. D. Bastiani, A. Giugni, B. Torre, E. D. Fabrizio, O. F. Mohammed, A. Rothenberger, T. Wu, A. Goriely, O. M. Bakr, *ACS Energy Lett.* **2017,** *2*, 1782.
[105] Y. Dang, D. Ju, L. Wang, X. Tao, *CrystEngComm* **2016,** *18*, 4476.
[106] Y. Liu, Z. Yang, S. F. Liu, *Adv. Sci.* **2018,** *5*, 1700471.
[107] N. J. Jeon, J. H. Noh, W. S. Yang, Y. C. Kim, S. Ryu, J. Seo, S. I. Seok, *Nature* **2015,** *517*, 476.
[108] J. J. Shi, J. Dong, S. T. Lv, Y. Z. Xu, L. F. Zhu, J. Y. Xiao, X. Xu, H. J. Wu, D. M. Li, Y. H. Luo, Q. B. Meng, *Appl. Phys. Lett.* **2014,** *104*, 063901.
[109] Y. Jin, G. Chumanov, *ACS Appl. Mater. Interfaces* **2015,** *7*, 12015.
[110] D. Liu, J. Yang, T. L. Kelly, *J. Am. Chem. Soc.* **2014,** *136*, 17116.
[111] W. Ke, G. Fang, J. Wan, H. Tao, Q. Liu, L. Xiong, P. Qin, J. Wang, H. Lei, G. Yang, M. Qin, X. Zhao, Y. Yan, *Nat. Commun.* **2015,** *6*, 6700.
[112] T. Ye, W. Fu, J. Wu, Z. Yu, X. Jin, H. Chen, H. Li, *J. Mater. Chem. A* **2016,** *4*, 1214.
[113] Y. Liu, X. Ren, J. Zhang, Z. Yang, D. Yang, F. Yu, J. Sun, C. Zhao, Z. Yao, B. Wang, Q. Wei, F. Xiao, H. Fan, H. Deng, L. Deng, S. F. Liu, *Sci. China Chem.* **2017,** *60*, 1367.
[114] H. S. Rao, B. X. Chen, X. D. Wang, D. B. Kuang, C. Y. Su, *Chem. Commun.* **2017,** *53*, 5163.
[115] Y. Li, L. Han, Q. Liu, W. Wang, Y. Chen, M. Lyu, X. Li, H. Sun, H. Wang, S. Wang, Y. Li, *Nano Res.* **2018,** *11*, 3306.
[116] H.-L. Yue, H.-H. Sung, F.-C. Chen, *Adv. Electron. Mater.* **2018,** *4*, 1700655.
[117] J. Zhao, G. Kong, S. Chen, Q. Li, B. Huang, Z. Liu, X. San, Y. Wang, C. Wang, Y. Zhen, H. Wen, P. Gao, J. Li, *Sci. Bull.* **2017,** *62*, 1173.
[118] Y. Huang, Y. Zhang, J. Sun, X. Wang, J. Sun, Q. Chen, C. Pan, H. Zhou, *Adv. Mater. Interfaces* **2018,** *5*, 1800224.
[119] Y. Liu, Q. Dong, Y. Fang, Y. Lin, Y. Deng, J. Huang, *Adv. Funct. Mater.* **2019**, 1807707.
[120] L. Lee, J. Baek, K. S. Park, Y. E. Lee, N. K. Shrestha, M. M. Sung, *Nat. Commun.* **2017,** *8*, 15882.
[121] H. S. Kim, I. H. Jang, N. Ahn, M. Choi, A. Guerrero, J. Bisquert, N. G. Park, *J. Phys. Chem. Lett.* **2015,** *6*, 4633.
[122] H. J. Snaith, A. Abate, J. M. Ball, G. E. Eperon, T. Leijtens, N. K. Noel, S. D. Stranks, J. T.-W. Wang, K. Wojciechowski, W. Zhang, *J. Phys. Chem. Lett.* **2014,** *5*, 1511.
[123] Y. Yuan, J. Huang, *Acc. Chem. Res.* **2016,** *49*, 286.

[124] A. A. Zhumekenov, M. A. Haque, J. Yin, A. M. El-Zohry, K. J. Lee, I. Dursun, O. F. Mohammed, D. Baran, O. M. Bakr, *J. Phys. D: Appl. Phys.* **2019,** *52*, 054001.
[125] C. Ortiz-Cervantes, P. Carmona-Monroy, D. Solis-Ibarra, *ChemSusChem* **2019,** *12*, 1560.
[126] B. E. Cohen, Y. Li, Q. Meng, L. Etgar, *Nano Lett.* **2019,** *19*, 2588.
[127] H. Tsai, W. Nie, J. C. Blancon, C. C. Stoumpos, R. Asadpour, B. Harutyunyan, A. J. Neukirch, R. Verduzco, J. J. Crochet, S. Tretiak, L. Pedesseau, J. Even, M. A. Alam, G. Gupta, J. Lou, P. M. Ajayan, M. J. Bedzyk, M. G. Kanatzidis, *Nature* **2016,** *536*, 312.
[128] X. Zhang, G. Wu, W. Fu, M. Qin, W. Yang, J. Yan, Z. Zhang, X. Lu, H. Chen, *Adv. Energy Mater.* **2018,** *8*, 1702498.
[129] T. Luo, Y. Zhang, Z. Xu, T. Niu, J. Wen, J. Lu, S. Jin, S. F. Liu, K. Zhao, *Adv. Mater.* **2019**, 1903848.
[130] Y. Zhang, P. Wang, M. C. Tang, D. Barrit, W. Ke, J. Liu, T. Luo, Y. Liu, T. Niu, D. M. Smilgies, Z. Yang, Z. Liu, S. Jin, M. G. Kanatzidis, A. Amassian, S. F. Liu, K. Zhao, *J. Am. Chem. Soc.* **2019,** *141*, 2684.
[131] K. Leng, I. Abdelwahab, I. Verzhbitskiy, M. Telychko, L. Chu, W. Fu, X. Chi, N. Guo, Z. Chen, Z. Chen, C. Zhang, Q. H. Xu, J. Lu, M. Chhowalla, G. Eda, K. P. Loh, *Nat. Mater.* **2018,** *17*, 908.
[132] Y. Liu, Y. Zhang, Z. Yang, H. Ye, J. Feng, Z. Xu, X. Zhang, R. Munir, J. Liu, P. Zuo, Q. Li, M. Hu, L. Meng, K. Wang, D. M. Smilgies, G. Zhao, H. Xu, Z. Yang, A. Amassian, J. Li, K. Zhao, S. F. Liu, *Nat. Commun.* **2018,** *9*, 5302.
[133] Y. Liu, H. Ye, Y. Zhang, K. Zhao, Z. Yang, Y. Yuan, H. Wu, G. Zhao, Z. Yang, J. Tang, Z. Xu, S. Liu, *Matter* **2019,** *1*, 465.
[134] H. S. Rao, W. G. Li, B. X. Chen, D. B. Kuang, C. Y. Su, *Adv. Mater.* **2017,** *29*, 1602639.
[135] Z. Yang, S. Zhang, L. Li, W. Chen, *J. Materiomics* **2017,** *3*, 231.

Author biographies and photographs

Azimul Haque is currently a Ph.D. student in OMEGALAB, Department of Materials Science & Engineering, KAUST. He received his bachelor's degree in Nanotechnology from SRM University (Chennai, India) in 2013. His current research interests include hybrid perovskite solar cells, photodetectors, lead-free hybrid materials and thermoelectrics.

Joel Troughton received his B.Eng in Materials Science from Swansea University, UK in 2011, followed by an Eng.D in 2016. Before joining OMEGALAB, KAUST in 2017 as a postdoctoral fellow, he worked as a technology transfer fellow at the Sustainable Product Engineering Centre for Innovative Functional Industrial Coatings (SPECIFIC, UK) developing up-scalable processing techniques for perovskite solar cells.

Derya Baran recieved her PhD from Friedrich-Alexander University Erlangen-Nurnberg, Germany in 2014. She worked at Jülich Forschungszentrum, Germany and Center for Plastic Electronics, Imperial College London, UK prior to joining KAUST as an Assistant Professor in 2017. Her research group, OMEGALAB focuses on solution processable organic/hybrid soft materials for electronic devices including solar cells and thermoelectric devices.

Table of contents

Optoelectronic devices based on single-crystalline halide perovskites have attracted significant attention owing to its superior quality over polycrystalline counterparts. This review summarizes the transition from large grain polycrystalline perovskite film-based solar cells to single-crystalline perovskite solar cells in different architectures.

Keywords: perovskite, grain, single crystal, solar cell

Md Azimul Haque, Joel Troughton, Derya Baran**

Processing-Performance Evolution of Perovskite Solar Cells: from Large Grain Polycrystalline films to Single Crystals

ToC figure